The eruptive chronology of the carihuairazo volcano (Ecuador): Recurrent sector collapses of a Middle Pleistocene stratovolcano of the northern andes

Pablo Samaniego, Jorge Ordóñez, Mathilde Bablon, Minard Hall, Xavier Quidelleur, Pierre Lahitte, Santiago Santamaria, Céline Liorzou

To cite this version:

Pablo Samaniego, Jorge Ordóñez, Mathilde Bablon, Minard Hall, Xavier Quidelleur, et al.. The eruptive chronology of the carihuairazo volcano (Ecuador): Recurrent sector collapses of a Middle Pleistocene stratovolcano of the northern andes. Journal of South American Earth Sciences, 2022, pp.103865. 10.1016/j.jsames.2022.103865 . hal-03689975

HAL Id: hal-03689975
https://hal.science/hal-03689975v1

Submitted on 22 Jul 2024

HAL is a multi-disciplinary open access archive for the deposit and dissemination of scientific research documents, whether they are published or not. The documents may come from teaching and research institutions in France or abroad, or from public or private research centers.

L'archive ouverte pluridisciplinaire **HAL**, est destinée au dépôt et à la diffusion de documents scientifiques de niveau recherche, publiés ou non, émanant des établissements d'enseignement et de recherche français ou étrangers, des laboratoires publics ou privés.

Distributed under a Creative Commons Attribution - NonCommercial 4.0 International License

Version of Record: https://www.sciencedirect.com/science/article/pii/S0895981122001559
Manuscript_98fb645d12657bd0d4fe64f31a4a4b80

The eruptive chronology of the Carihuairazo volcano (Ecuador): recurrent sector collapses of a Middle Pleistocene stratovolcano of the Northern Andes

Pablo Samaniego[1], Jorge Ordóñez[2,*], Mathilde Bablon[3,4], Minard L. Hall[2],
Xavier Quidelleur[4], Pierre Lahitte[4], Santiago Santamaria[2,4], Céline Liorzou[5]

[1] Université Clermont Auvergne, CNRS, IRD, OPGC, Laboratoire Magmas et Volcans, F-63000 Clermont-Ferrand, France

[2] Instituto Geofísico, Escuela Politécnica Nacional, Ladrón de Guevara E11-253, Ap. 2759, Quito, Ecuador

[3] Université Côte d'Azur, Observatoire de la Côte d'Azur, CNRS, IRD, Géoazur, 250 rue Albert Einstein, Sophia Antipolis 06560 Valbonne, France.

[4] Université Paris-Saclay, CNRS, Laboratoire GEOPS, Rue du Belvédère, 91405 Orsay, France

[5] Laboratoire Géosciences Océan, Institut Universitaire Européen de la Mer, Université de Bretagne Occidentale, Rue Dumont d'Urville, 29280 Plouzané, France

Corresponding author: pablo.samaniego@ird.fr

* Now at: Dirección Metropolitana de Gestión de Riesgos, Secretaria de Seguridad y Gobernabilidad, Municipio de Quito

Manuscript submitted to the Journal of South American Earth Sciences

© 2022 published by Elsevier. This manuscript is made available under the CC BY NC user license
https://creativecommons.org/licenses/by-nc/4.0/

Abstract

The eruptive chronology of arc volcanoes consists of construction stages usually punctuated by large collapse events affecting the edifice. In this paper, we reconstruct the eruptive chronology of Carihuairazo volcano, a Middle Pleistocene edifice from the Ecuadorian segment of the Andean Northern Volcanic Zone. This study is based on extensive fieldwork on both the proximal flanks of the volcano and the medial-to-distal deposits of the nearby Ambato basin, as well as a large dataset of geochronological (^{40}K-^{40}Ar, ^{14}C) and geochemical (major and trace element) data. The Basal Carihuairazo edifice is mainly composed of an andesitic lava flow succession dated at 230-200 ka. The resulting edifice suffered a first sector collapse that was responsible for a relatively large (4 ± 1 km^3) debris avalanche deposit (DAD-1) that covers the entire Ambato basin. This event occurred between 206 ± 4 and 216 ± 5 ka. Then, Carihuairazo started a succession of construction (Intermediate and Terminal lava flow successions) and destruction stages lasting about 50 ky (*i.e.*, from 200 to 150 ka), which are composed by thick block-and-ash flow deposits (L- and U-BAFD) and debris avalanche deposits (DAD-2). This volcanic succession is recorded in the Ambato basin, interlayered with several tephra fallout deposits (TFD-1 to -4) whose source is the neighbouring Huisla-Mulmul volcanic complex. The current morphology of Carihuairazo results from two additional sector collapses (DAD-3 and -4) that occurred during the past 40-50 ka, *i.e.*, following a long period (at least 100 ka) without volcanic activity. We stress these debris avalanches were not related with magmatic activity. Samples from the Carihuairazo volcano defines a medium-K magmatic trend composed of andesites and dacites with a mineral assemblage of plagioclase, amphibole, ortho- and clino-pyroxene, and Fe–Ti oxides. The evolution of the Carihuairazo edifice, recorded in the medial-distal deposits of the Ambato basin, represents a unique example in the Ecuadorian arc of an edifice that experienced successive destruction and construction stages during a major part of its volcanic history.

Keywords: eruptive chronology, debris avalanche deposits, unspiked K-Ar dating, Carihuairazo, Ecuador

1. Introduction

The eruptive chronology of composite volcanoes often consists of long-lasting growth stages punctuated by collapse events affecting a single flank or the entire edifice. These destabilization events may produce large volcanic landslides that usually transform into long runout debris avalanches (van Wyk de Vries and Davis, 2015). In addition, some edifices are capped by lava domes complexes that are intrinsically prone to gravitationally-controlled collapse events (Calder et al., 2015). The resulting debris avalanches and dome-collapse deposits, emplaced at medial to distal locations at the foot of the composite volcanoes, provide a detailed stratigraphic record that can help to define the succession of construction and destruction stages of stratovolcanoes (Zemeny et al., 2021). In the Ecuadorian Andean context, volcanic sector collapses often occur during volcanoes' lifetime, with some well-studied examples for large sector collapses at Chimborazo (Bernard et al., 2008; Samaniego et al., 2012), Tungurahua (Hall et al., 1999; Bablon et al., 2018), and Sangay (Monzier et al., 1999; Valverde et al., 2021). However, there are no detailed studies of volcanoes that experienced recurrent sector collapses followed by reconstruction episodes involving dome complex activity during a relatively short time span. This scenario has been described in other edifices such as Taranaki in New Zealand (Zemeny et al., 2021), Shiveluch in Kamchatka (Belousov et al., 1999), Colima in Mexico (Robin et al., 1987), or Tutupaca in Peru (Samaniego et al., 2015; Mariño et al., 2021).

The Ecuadorian province of the Andean Northern Volcanic Zone (NVZ) is characterized by a large number (up to 85) of Late Quaternary volcanic centres distributed in a quite small arc segment of less than 300 km-long (Fig. 1a). This volcanic arc results from the subduction of the oceanic Nazca plate below the South American continental plate (Fig. 1b). The Ecuadorian volcanoes are distributed along north-south alignments that follow the different morphological units composing the Ecuadorian Andes: the Western Cordillera, the Inter Andean Valley, the Eastern Cordillera, and the Sub-Andean zone (Hall et al., 2008). The southern termination of the NVZ is a triangular-shaped arc segment located in central Ecuador, around the cities of Ambato and Riobamba, and it includes large volcanic centres such as Chimborazo (Samaniego et al., 2012), Tungurahua (Hall et al., 1999; Bablon et al., 2018) and Sangay (Monzier et al., 1999). Based on a regional study, Bablon et al. (2019) proposed that this part of the NVZ developed during the last 0.6 Ma due to the evolving geometry of the slab below this part of the arc (Yepes et al., 2016; Araujo et al., 2021) and the activation of major crustal faults (Baize et al., 2020).

Figure 1. (a) The Quaternary Ecuadorian volcanic, including some of the most important edifices (from Hall et al., 2008) as well as the main active faults (from Alvarado et al., 2014). **(b)** Geodynamical setting of the Ecuadorian arc. GFZ: Grijalva Fracture Zone; GSC: Galápagos Spreading Center; Ca : Carihuairazo. Edifices cited in the text (dark grey): (1) Mojanda-Fuya Fuya, (2) Imbabura, (3) Cubilche, (4) Pichincha, (5) Cotopaxi, (6) Sagoatoa, (7) Chimborazo, (8) Puñalica, (9) Huisla-Mulmul, (10) Tungurahua, (11) Sangay. Main cities: Q, Quito, I, Ibarra; L, Latacunga; A, Ambato; R, Riobamba.

The eruptive chronology of the large and most active edifices of the southern termination of the Ecuadorian arc has been reconstructed during the last two decades (see references above). However, little is known about other volcanoes, such as Carihuairazo (78°45'W, 01°24'S, 5018 m above sea level -asl), which is located ~140 km south of the Ecuador's capital city, Quito, and only 20 km south-west of Ambato (Fig. 1a). This volcano, together with the nearby Chimborazo and Puñalica, are constructed on top of the Western Cordillera of the Ecuadorian Andes, which is composed of Cenozoic volcano-sedimentary sequences formed in marine environments, and younger Miocene and Pliocene continental arc-related volcanic sequences (Hughes and Pilatasig, 2002; Jaillard et al., 2004).

The Carihuairazo volcano overlooks the Ambato basin, a densely populated tectonic depression forming the central-southern part of the Inter Andean valley. In this context, reconstructing the eruptive chronology of this edifice represents a crucial step of any hazard assessment strategy. In this work, we coupled detailed stratigraphic data, geomorphometric reconstructions, geochronological information and geochemical analyses to define the eruptive chronology and the construction/destruction stages of the Carihuairazo volcano during the Middle Pleistocene.

2. Analytical methods

Several field trips were performed in 2009-2011 and included geological mapping and sampling of most stratigraphic units, especially for the Ambato basin distal deposits (Ordóñez, 2012). Additional fieldwork on proximal areas was performed in 2016-2019. As a result, we now have a large (82) sample array of lavas and tephras covering most volcanic units that allow us to reconstruct the volcanological evolution of the Carihuairazo volcano.

2.1. Major and trace elements whole-rock analyses

Major and trace elements analyses were obtained at the Laboratoire Géosciences Océan (Université de Bretagne Occidentale, Brest, France) from agate-crushed powders of 82 new samples spanning the entire volcanic history of Carihuairazo volcano and the Ambato basin deposits (Table 1). We used an Inductive Coupled Plasma-Atomic Emission Spectrometer (ICP-AES), following the analytical procedure described by Cotten et al. (1995). In addition, to proceed with stratigraphic correlations, we also used published data from the neighbouring Puñalica (Narvaez et al., 2018), Huisla-Mulmul and Chimborazo volcanoes (Samaniego et al., 2012; Ancellin et al., 2017).

2.2. Radiometric dating

The chronology of the Middle Pleistocene eruptive activity was established using the unspiked K-Ar dating technique. Nine new age determinations were obtained at Geoscience Paris-Saclay (GEOPS) laboratory, which complement the six ages previously obtained by Samaniego et al. (2012) and Bablon et al. (2019). Lava flows and juvenile blocks of pyroclastic currents deposits were selected based on their freshness and low vesicle content. The ages of these samples were calculated by measuring their potassium and radiogenic argon (^{40}Ar*) content and using the ^{40}K/K ratio and the ^{40}K radioactive decay constants of Steiger and Jäger (1977). We used the unspiked Cassignol-Gillot technique applied to groundmass and plagioclase (Cassignol and Gillot, 1982; Gillot et al., 2006), which is well-suited for Quaternary volcanic products containing low ^{40}Ar* contents, and that has already been successfully applied in Ecuador (Bablon et al., 2018; 2019; Santamaria et al., 2022), as well as in other volcanic arcs worldwide (*e.g.,* Germa et al., 2011; Grosse et al., 2018; Lahitte et al., 2019). The ^{40}Ar* content is derived from comparing the ^{40}Ar/^{36}Ar ratios of the sample and the atmosphere. Therefore, the apparent age corresponds to the age of the eruption when measurements are performed on groundmass, or on juvenile crystals. Otherwise, the apparent age could be older than the eruption, biased by the inherited or excess ^{40}Ar trapped in the phenocrysts that were not reset in the magma reservoir before eruption (*e.g.,* Harford et al., 2002; Samper et al., 2008; Germa et al., 2019).

To extract the freshest groundmass, the selected samples were crushed and sieved in the 80-125 or 125-250 µm size-fraction depending on the size and proportion of phenocrysts. Groundmass or alternatively plagioclase crystals (*e.g.*, samples 16EQ31 and CAR69; Table 2), were isolated by heavy liquids and magnetic separations to obtain fractions of homogeneous density ($d_{avg} \approx 2.65$). Potassium and argon measurements were duplicated to check their reproducibility within 1-σ uncertainty. Potassium contents were calculated using reference values of MDO-G (K = 3.510%; Gillot et al., 1992) and BCR-2 (K = 1.481%; Raczek et al., 2001) standards, and $^{40}Ar^*$ contents were routinely checked by measurement of ISH-G (1301-1302 AD; Gillot et al., 1992) and HD-B1 (24.21 ± 0.32 Ma; Hess and Lippolt, 1994) standards. More details about the sample preparation, analytical procedures and uncertainties calculation are provided in Bablon et al. (2018).

Lastly, the Late Pleistocene chronology of the volcanic explosive activity in this region was constrained by three new radiocarbon ages (Table 3) obtained from charcoal samples collected from distal deposits of the Ambato basin. These samples were analysed at the Centre for Isotope Research (CIO, Groningen University, Netherlands). Before ^{14}C measurement, samples were examined under a binocular microscope with the aim of eliminating any potential contaminant such as sand and roots. Then, the samples were chemically pre-treated to remove contaminants, in order to isolate a suitable fraction for dating. The performed treatment (referred as "AAA") consists of the following steps: (1) acid (HCl) leaching to remove soil carbonate; (2) alkali (NaOH) leaching to remove humic acids; and, (3) acid (HCl) leaching to remove any "modern" CO_2 absorbed during the previous steps. Variable amounts of the dried sample were used to obtain, after combustion, a CO_2 volume equivalent to at least 1 mg of C. Then, CO_2 is reduced by H_2 in the presence of iron powder. ^{14}C activity is finally measured by mass spectrometry. The ^{14}C ages are calculated following the procedure of Mook and van der Plicht (1999) and corrected for mass dependent effects (isotope fractionation) using the measured $^{13}C/^{12}C$ ratio.

2.3. Geomorphological reconstruction

Numerical reconstructions of the temporal evolution of paleo-surfaces were used to estimate the volume of material emitted during the construction of Carihuairazo volcano (V_c) and the volume of eroded material (V_e) since the end of its activity. Such volumes ($V = \int_{u.a.} \Delta_Z \times ds$) correspond to the elevation difference between the upper and the lower surfaces encompassing any unit/edifice ($\Delta_Z = Z_{upper} - Z_{lower}$), integrated over the area (ds) of the given unit/edifices (u.a.). Considering the duration of their respective activity (ΔT_c) and quiescence (ΔT_e) periods, we can then quantify their eruptive (output) and erosion rates ($OR = \frac{Vc}{\Delta \mathrm{T}_c}$ and $ER = \frac{Ve}{\Delta \mathrm{T}_e}$, respectively). We extracted the present volcano elevation data from a 30-m SRTM Digital Elevation Model (DEM), and we used the reconstruction method using the ShapeVolc algorithm developed in Lahitte et al. (2012) and improved in Bablon et al. (2018) and Dibacto et al. (2020). The paleo-topography at the end of the construction of Carihuairazo is modelled from the extrapolation of elevation points extracted from the current crests, and assumed to belong to non-eroded surfaces. The topography prior to the construction of Carihuairazo was modelled by extrapolating the present basement elevation around the volcano, using the conventional kriging algorithm. The volume uncertainty is defined by the integration of the elementary uncertainty of height differences over the edifice area (u.a.) as $\sigma_\mathrm{V} = \sigma_\mathrm{Z} \times u.a.$, where the uncertainty of the elevation (σ_z) is $\sigma_z = \sqrt{{\sigma_{Z_{upper}}}^2 + {\sigma_{Z_{lower}}}^2}$. The average uncertainty of the surface elevation is estimated to be 200 m for the basement from the error maps generated with kriging interpolation, and to be 20 m for the surface models, based on the standard deviation of the elevation dispersion of the surfaces used for extrapolations around the surface modelled by ShapeVolc reconstruction. Finally, the rate uncertainty is defined as $\sigma_R = R\sqrt{\left(\frac{\sigma_V}{V}\right)^2 + \left(\frac{\sigma_T}{\Delta T}\right)^2}$, where R is the eruptive or erosion rate, $\frac{\sigma_\mathrm{V}}{\mathrm{V}}$ the relative uncertainty of the erupted or eroded unit/edifice volume and $\frac{\sigma_\mathrm{T}}{\Delta \mathrm{T}}$ the relative uncertainty of the duration of the activity or quiescence period, calculated from K-Ar ages uncertainties (Table 2).

3. Morphology and structure

Carihuairazo edifice displays a roughly circular basal outline (14-15 km in diameter) and a summit (5018 m above sea level - asl) located on the south-western part of the edifice. The asymmetrical shape originates from its location between the Inter Andean valley to the east and the high-plateau of the Western Cordillera to the west (Fig. 1-4). As a result, the base of the volcano is located at 3200-3300 m asl in the eastern side, and 3900-4000 m asl in the western side. Longitudinal valley profiles also show a higher elevation for rivers located on the western side (*i.e.*, A, I; Fig. 4a, b), and those of the north-eastern (*i.e.*, C, D, E; Fig. 4a, b), and eastern (*i.e.*, G; Fig. 4a, b) sides, related to the basement elevation offset. The lower flanks of Carihuairazo (below 4500 m asl) show gentle slopes (<10º), whereas at higher altitudes an uneven topography with steep slopes (10-30º, Fig. 2a) is observed. The summit zone is characterised by a 1-2 km-wide east-opened scar that is drained by the Pachanlica valley (Fig. 2b-c, 3). Other large (200-300 m depth) U-shaped glacial valleys with steep sides and flat bottom have also been carved around the edifice (Fig. 4c), containing arcuate, 2-3 km-long, 100-200 m-high outer and/or terminal moraines (Fig. 2d). In addition, just to the north of the Pachanlica valley, the Puñalica volcano (3988 m asl), a small (400-600 m-high), young-looking cone (Fig. 1, 2e) stands on the remnants of the lower north-east flank of Carihuairazo. Puñalica has a basal diameter of *c.* 3-4 km and a summit slightly elongated in a NW-SE direction, that includes several coalescent craters. Glacial erosion did not affect Puñalica, suggesting a post-glacial age younger than the Last Glacial Maximum (LGM).

From the morphology of the Chimborazo and Carihuairazo volcanoes, different authors (Clapperton, 1990; Samaniego et al., 2012) identified three successive groups of moraines that were assigned to the LGM, the Younger Dryas (YD) and the younger Neo-Glacial (NG) periods. At Carihuairazo, the oldest moraines extended down to 3200-3300 m asl in the northern and eastern flanks. Based on ^{14}C ages obtained from peat layers under and overlying these moraines, Clapperton (1990) proposed an age ranging between *ca.* 33 and 14 ka for the LGM moraines in this part of the Andes. Recently, Bablon et al. (2019) dated a lava sample from Chimborazo volcano (Guano lava flows of Samaniego et al., 2012) that yielded an age of 30 ± 3 ka (sample 16EQ43). This lava unit is covered by thick moraine deposits interpreted by Samaniego et al. (2012) as associated with the LGM period. Based on this evidence, we conclude that the moraines ascribed to the LGM in this part of the Andes are younger than 30 ± 3 ka, roughly corroborating the age range proposed by Clapperton (1990). Other intermediate moraines are radially distributed around Carihuairazo forming sequences of 3-4 arcuate moraines reaching 3700-3900 m asl (Fig. 2d). Whether or not this intermediate moraine sequence corresponds to the Younger Dryas period is beyond the scope of this study. However, our observations suggest that many glacial advances occurred in this part of the Andes between 30 and 10 ka.

Interestingly, a conspicuous break-in-slope is observed at about 3700-3900 m in the glacial valleys on the north, south and south-east flanks of the volcano (see Fig. 3, 4b). This morphological change is interpreted as resulting from the lower limit of glacial erosion associated with the LGM. Lastly, above 4400-4500 m asl, we observed smaller moraines that, following Clapperton (1990), should correspond to the Holocene glacial advances (the so-called Neo-Glacial period).

Figure 2. Panoramic views of the Carihuairazo volcano. The view directions are shown in Fig. 3. **(a)** View from the west showing the Carihuairazo basal lavas and the summit lavas and breccias. **(b)** View from the east, showing the Pachanlica valley which is partially filled with the post-glacial deposits related to the 1698 *CE* mudflow. **(c)** Oblique aerial view from the north, showing the Carihuairazo summit, the Pachanlica valley and the remnants of the last sector collapse that affected the north-western flanks of Carihuairazo (red dashed line). DFD: debris flow deposits. **(d)** Quebrada Chiquicahua valley at the northern flank of Carihuairazo. This deep valley was probably formed during the LGM glaciations. At least three moraines crop out in the valley's flank, probably associated with the YD period (white dashed lines). Note also the 1698 *CE* mudflow deposits at the valley's bottom and the small escarpment along the valley (black dotted line). **(e)** The young-looking Puñalica cone was constructed on top of old volcanic deposits and LGM moraines.

4. Volcanic stratigraphy of Carihuairazo volcano

4.1. The Carihuairazo edifice

Old lava domes. Two isolated, highly eroded lava domes crop out on the northern flank of the volcano, 8 km from the current summit (*e.g.*, Sunantza and Cruz Maqui; dark green unit, Fig. 3). Their morphology suggests that they are older structures that are not associated with the adjacent NE-elongated crests of the Yanasacha sector (Fig. 3). A K-Ar age obtained from the Sunantza andesitic lava dome yielded an age of 512 ± 9 ka (CAR14, Bablon et al., 2019). Based on this age and the morphological information, we argue that these pyroxene-bearing siliceous andesitic (59.6-63.0 wt.% SiO_2) lava domes correspond to the oldest volcanic unit of the Carihuairazo edifice.

Basal lava flows. This unit comprises a succession of massive (50-80 m-thick) lava flows from the northern, western, and southern flanks of Carihuairazo, roughly from the base of the volcano up to 4500-4600 m asl (dark brown unit, Fig. 3). This unit consists of a 400-600 m-thick andesitic lava pile (59-61 wt.% SiO_2). The oldest ages from this unit correspond to the thick lava flows of the lower south-west (Loma Piedra Negra) and south-east flanks that yielded $^{40}Ar/^{39}Ar$ plateau ages ranging from about 200 to 230 ka (Fig. 3; Samaniego et al., 2012), with two samples from the south-east flank dated at 221 ± 5 and 224 ± 5 ka (RIO117 and RIO118, respectively), and two samples from the south-west flank dated at 213 ± 5 and 208 ± 10 ka (RIO87A and B, respectively). These basal lava flows form the Abraspungo saddle between Carihuairazo and Chimborazo volcanoes. In the upper proximal zone, the oldest age corresponds to a lava flow intercalated on a lava flows and breccia succession that forms the inner scar wall, in the north-east flank of the edifice. This andesitic lava flow, dated here at 217 ± 9 ka (16EQ45, Table 2; Fig. 3), is undistinguishable from the previously mentioned $^{40}Ar/^{39}Ar$ ages from the outer flanks.

Chibuleo block-and-ash-flow deposits. In the northern part of the volcano, the flat surfaces of Chibuleo, Pilahuin, and Tambo Loma are made of a thick succession of several block-and-ash-flow deposits that rest on the Carihuairazo Basal lava flows and on the Plio-Quaternary volcanic sequence exposed on the Río Ambato valley (dark yellow unit, Fig. 3). These reddish-grey, structureless deposits have individual thicknesses of 10-15 m, and are composed of large blocks (>1-2 m in diameter) within a sand-rich matrix (60-70 vol.%). The juvenile blocks are amphibole-bearing siliceous andesites (60.8-62.8 wt.% SiO_2). This block-and-ash-flow succession was likely produced during a large dome-forming phase at Carihuairazo, whose dome remnants were not identified. This unit is overlain by a thick (up to 50 m) succession of weathered tephra fallout deposits with intercalated, partially indurated and reworked ash-rich layers (locally named Cangahua). At the base of this tephra fallout succession, we identified a 1-m-thick pumice-rich layer that consists of white, rhyolitic pumice erupted from the Huisla-Mulmul volcanic complex (TFD-1, see below).

Figure 3. Geological sketch map of the Carihuairazo volcano, including the location of the new (white) and previous (grey) dated samples (ages in ka). Previous ages come from Samaniego et al. (2012) and Bablon et al. (2019). Grey colours for surrounding areas: dark grey for the Mio-Pliocene volcanic sequences, light grey for neighbouring volcanoes. The points of view refer to Fig. 2.

Figure 4. **(a)** Shaded relief view of the 4-m DEM of Carihuairazo and Puñalica volcanoes, with main rivers highlighted by different colours. **(b)** Longitudinal profile of rivers plotted from the high point of the Carihuairazo elevation model at the end of its construction. Same colours as Fig. 4a. **(c)** Transverse profile of rivers. Cross sections and associated colours are indicated in Fig. 4a. **(d)** Shaded relief view showing the elevation of crests used to compute paleo-topographies of the volcano.

Intermediate lava flows and breccias. This unit is composed by a thick succession of lava flows and breccias conforming the outer western and south-western flanks, above a marked break-in-slope at around 4500 m asl (light green unit, Fig. 3). These thick andesitic lavas overlay the Basal lava flows (*i.e.* Piedra Negra). We obtained two similar ages of 199 ± 5 and 198 ± 7 ka (16EQ49 and 16EQ51, respectively; Table 2) from this lava flow succession, which are slightly younger than the previously described Basal lava flows. This intermediate unit is also formed by the monotonous lava flow succession conforming the north-eastern crests (i.e. Yanasacha) located between the

Quebrada (ravine) Chiquicahua and Quebrada Quichibi. Two similar ages were obtained from the north-eastern (197 ± 4 ka, groundmass age of 16EQ31; Table 2) and northern flanks (186 ± 5 ka; CAR69; Table 2 and Fig. 2a-b, and 3). Note that 16EQ31 sample was also dated at 187 ± 9 ka on plagioclase crystals. However, because their K content is four times lower than that of the groundmass, we only consider here the best-constrained age of 197 ± 4 ka. We stress these ages are slightly younger than that of the Basal lava flows succession ranging from 224 ± 5 to 208 ± 10 ka (Samaniego et al., 2012).

We include in this unit the non-continuous, heterogeneous, hydrothermally-altered lavas and breccias successions cropping out along the Pachanlica valley (*i.e.* Milincocha hill). We interpret this sequence as a series of "toreva" megablocks associated with the first large sector collapse that affected the Carihuairazo (DAD-1, see below; Fig. 3).

Terminal lava flows. The upper remnants of the Carihuairazo cone are composed of a succession of amphibole-bearing andesitic (59-60 wt.% SiO_2) lava flows with interlayered breccias (light brown-red unit, Fig. 3). Two ages were obtained on this succession, yielding ages of 172 ± 7 and 157 ± 5 ka (16EQ50 and 16EQ48, respectively; Table 2). Compared with the Basal/Intermediate lava flows, this lava succession displays higher slopes that mark a clear angular discordance. However, given the lack of a conspicuous erosional discordance between the Basal and Intermediate lava flows units and the Terminal lava flows, and the overlapping radiometric ages for Intermediate and Terminal units, we propose that the construction of the Terminal edifice followed the Intermediate lavas by only a few thousands of years.

We include in this unit the amphibole-bearing dacitic domes (Santa Rosa, Cahuito and Pitiunga) that crop out on both sides of the Pachanlica valley (Fig. 2c, 3). An additional age was obtained from the Pitiunga dome, yielding an age of 176 ± 10 ka (CAR60, Table 2) which is identical to that of the lavas from the upper remnants of Carihuairazo.

4.2. Stratigraphy of the Ambato basin

In this section we describe in a stratigraphic order, the debris avalanche and the pyroclastic currents deposits of the Ambato basin. Based on stratigraphic and morphological considerations, as well as geochemical characteristic of the juvenile products (see below), these deposits originated from the Carihuairazo volcano. We also describe the regional tephra fallout deposits that are interlayered in this volcanic succession. The Ambato basin volcanic succession overlies the Quaternary volcano-sedimentary deposits of the Inter Andean valley (the so-called Latacunga Formation, Lavenu et al., 1992) and the Chalupas ignimbrite deposits (Beate et al., 2006). It is worth noting that Bablon et al. (2019) obtained an age of 799 ± 12 ka for a lava flow from the Sagoatoa volcano, which is interlayered in the volcaniclastic deposits of the Latacunga Formation. In addition, the Chalupas ignimbrite deposits were recently dated at 216 ± 5 ka (Bablon et al., 2020). These ages, especially that of Chalupas deposits, represent the oldest bound for the Carihuairazo deposits in the Ambato basin. The detailed stratigraphic sections throughout the Ambato basin, and some key photos of the main units are shown in Fig. 5 and 6; whereas the synthetic stratigraphy of the Ambato basin is presented in Fig. 7.

Debris avalanche deposit 1 (DAD-1). This unit is exposed in the Ambato basin, from J.B. Vela to the west to the Totoras town to the east, mostly on the south side of the Río Ambato valley (Fig. 3). This deposit has a maximum runout of 25 km from its supposed source region on the upper flanks of Carihuairazo. Its south-east limit is not well constrained given that the younger lava flows from the Puñalica volcano overlay the DAD-1 south of Quebrada Catequilla (Fig. 3, 6). The greatest thickness was observed in the south-eastern part of the Ambato basin, reaching 25-40 m along the Río Mocha valley. In contrasts, in the north and north-eastern limit, the maximum observed thickness are of 5-10 m. Assuming an average thickness of 20 ± 5 m over about 200 km^2 (Fig. 8), the volume of DAD-1 is estimated at 4 ± 1 km^3.

The DAD-1 unit is composed of a massive, heterogeneous, polymictic breccia that, following the terminology of Glicken (1991), is composed of two facies deposits. The block facies consist of large (up to 2 m in diameter), highly cataclased blocks with abundant jigsaw cracks and fractures included in a sandy matrix. Lava blocks are mostly unaltered andesites with a mineral assemblage composed of plagioclase, pyroxenes, and amphibole, with some scarce hydrothermally-altered andesitic blocks. The mixed facies is composed of heterogeneous, beige, sand-rich interclast matrix (70-80 vol.%), with heterogeneous blocks (up to 20 cm in diameter) of similar composition than those from the block facies. The mixed facies is mainly observed at the lower part of the deposit. This unit overlays the volcaniclastic sediments of the Latacunga Formation, and the Chalupas ignimbrite deposits. This unit is covered by a thick rhyolitic tephra fallout deposit (TFD-1) and the lower block-and-ash flow deposits (L-BAFD) (Fig. 6).

Figure 5. **(a)** Bellavista quarry shows an almost complete cross-section for the Ambato basin. **(b)** La Peninsula, Rio Ambato valley. Contact between the Chalupas ignimbrite deposit and the DAD-1. **(c)** San Vicente quarry. **(d)** Juvenile block (with prismatic jointing) in the L-BAFD, San Vicente quarry. This block was dated by the K-Ar method (16EQ51, Table 2). **(e)** El Carmen quarry. **(f)** Small quarry on the Paso Lateral. Locations are indicated in Fig. 6, and abbreviations are detailed in Fig. 7 and in the text.

Lower block-and-ash-flow deposits (L-BAFD). In the north-western part of the Ambato basin, we observe a 100-300-m-high, NE-SW elongated relief made by the Casigana and Bellavista hills (Fig. 3). At the Bellavista and San Vicente quarries (Fig. 5, 6), this unit consists of at least three, 3-6 m-thick layers, of a matrix-supported (70-80 vol.%), monolithological breccia composed of angular blocks (up to 50-80 cm in diameter) included into a sandy, grey to reddish matrix. Juvenile blocks from these deposits are amphibole-bearing siliceous andesites (62-63 wt.% SiO_2). The upper half of each layer displays a reddish colour whereas the lower half mostly displays grey colour. Small charred organic material on this deposit that yielded ^{14}C age older than the method limit (>45 ka, Table 3). K-Ar dating of a juvenile prismatically-jointed block from this unit yielded an age of 206 ± 4 ka (17EQ115, Fig. 5d, Table 2). These block-and-ash-flow deposits are likely associated with the growth of a dome complex in the summit area. This unit is interlayered between the DAD-1 and the intermediate DAD-2 (see below; Fig. 6 and 7). Its upper and lower contacts are concordant, suggesting a deposition with a short lifespan between each unit.

Debris avalanche deposit 2 (DAD-2). This unit crops out at the north-western (Bellavista and San Vicente quarries) and south-eastern (El Carmen quarry) sides of the Ambato basin (Fig. 6). Because of its intermediate stratigraphic position, outcrops are scarce and we cannot fully define its geographical extension. Its thickness varies from 5-6 m up to 12 m across the Ambato basin, which should be considered as minimum values as its base was often not observed. Ordóñez (2012) proposed an area of 100 km^2 (Fig. 8), and, assuming an average thickness of 5-10 m, we propose a volume range of 0.5-1.0 km^3. Despite this rough estimation, DAD-2 exhibits a volume notably smaller than the older DAD-1. This unit overlies the TFD-1 (Totoras log, Fig. 6) and the lower block-and-ash flow unit (Bellavista log, Fig. 6), and it is covered by a tephra fallout deposit (TFD-2; El Carmen log, Fig. 6) and/or the upper block-and-ash flow unit (U-BAFD, Bellavista log, Fig. 6).

DAD-2 is a heterogeneous breccia showing a characteristic patchwork pattern, consisting of block facies immersed in a mixed facies (Fig. 5, 6). The block facies consists of large (up to 1-2 m in diameter), variably cataclased blocks with frequent jigsaw cracks and fractures immersed in a sandy matrix. Lava blocks are mostly unaltered andesites with a mineral assemblage composed of plagioclase, pyroxenes, and amphibole. The mixed facies is composed of heterogeneous, beige, sand-rich interclast matrix (60-70 vol.%), with primarily angular andesitic blocks (up to 20 cm in diameter) and some scarce pumice fragments from the lower TFD-1 horizon.

Figure 6. Key stratigraphic columns in the Ambato basin.

Upper block-and-ash-flow deposits (U-BAFD). This unit crops out in the basin's north-western side, at Bellavista and San Vicente quarries (Fig. 6, 7). This 6-8 m-thick unit is a matrix-supported (70-80 vol.%), monolithological breccia composed of angular blocks (up to 1-2 m in diameter) immersed in a sand-rich matrix with the characteristic grey-reddish colour. Juvenile blocks from this unit are amphibole-bearing siliceous andesites (62-63 wt.% SiO_2). This unit is concordant above the previously described DAD-2 and is covered by a tephra fallout deposit (TFD-2, El Carmen log, Fig. 6) and a younger debris avalanche deposit (DAD-3, logs San Vicente and Bellavista, Fig. 6). At El Carmen quarry, the upper part of U-BAFD grades into a 20-30 cm-thick, dark grey, ash-rich layer, interpreted as a paleosoil (see below). This paleosoil horizon is associated with an unconformity representing a period without volcanic deposition in the Ambato basin.

Debris avalanche deposit 3 (DAD-3). This unit is widely distributed in the Ambato basin. Good exposures occur along the main drainages (Fig. 3), *i.e.* the Quebradas Catequilla and Terremoto, and the Río Ambato and Río Pachanlica valleys, with a maximum runout of 25 km in the NE direction (DAD-3; Fig. 8). The observed thickness ranges from 2-5 up to 15-20 m. It covers an area of 100-110 km^2, quite similar to that of the DAD-2. The average thickness of 8-10 m leads to an estimated volume of ~1 km^3, a value similar to the DAD-2 and notably lower than DAD-1. This deposit is massive with no gradation structure. It is a heterogeneous, polymictic breccia, with the two typical facies observed in the previously described DADs. The block facies consists of large (up to 5 m in diameter), highly cataclased blocks with abundant jigsaw cracks and fractures immersed in a sandy matrix. Some scarce megablocks (200-250 m long and 20-50 m high) were observed and mainly consist of block facies. Lava blocks are mostly unaltered andesites with a similar mineral assemblage to those of the previously DADs. The mixed facies is composed of heterogeneous, beige, silty-sandy interclast matrix (75-85 vol.%), with heterogeneous blocks (up to 20 cm in diameter) of similar composition than in the block facies. The dominant mixed facies includes patches of the block facies. Lastly, a third, transitional facies was observed at the NE distal parts (e.g., Totoras). This polymictic deposit is characterised by a beige sandy-silty interclast matrix (50-65 vol.%) and includes subrounded blocks of andesitic composition. The matrix is consolidated and includes frequent millimetric-size bubbles. Based on these characteristics, and following the criteria summarized by Harpel et al. (2011), we interpret this subunit as a lahar deposit associated with the main debris avalanche deposit. The DAD-3 unit is interlayered between U-BAFD and TFD-2 units below and the TFD-3 unit above (Fig. 6).

Figure 7. Synthetic stratigraphy of the Ambato basin.

Figure 8. Debris Avalanche Deposits distribution in Ambato basin.

Debris avalanche deposit 4 (DAD-4). This unit is the youngest debris avalanche deposit of the Carihuairazo volcano. Contrary to the previous debris avalanche deposits that spread over a wide area of the Ambato basin, this unit is channelized along the Pataló, Terremoto and Catequilla valleys (Fig. 8). Its thickness is lower than the previous deposits, ranging from 1 to 5 m in the distal zone, and 8-12 m in the proximal zone (log 2, Río Pataló, Fig. 6). Ordóñez (2012) proposed an area of 65-70 km^2 for DAD-4 (Fig. 8), and assuming an average thickness of 2-3 m, we estimate a volume of 0.15-0.20 km^3.

This unit is a massive, polymictic, matrix-supported breccia composed of 10-20 vol.% of blocks, whose size ranges from 5 and 80 cm in diameter, although larger blocks (up to 1-2 m) were also observed. Blocks are primarily angular or subangular, with frequent jigsaw fractures, especially in larger blocks. The silt-rich matrix is commonly beige-brown, although in some cases, red-grey colours are also observed, and display frequent millimetric-size bubbles, especially at the base of the deposit. Blocks are primarily pyroxene-rich and amphibole-bearing andesites, mostly unaltered, although hydrothermally-altered blocks were also observed. The polylithologic nature of the blocks, the matrix's characteristics, and the presence of block facies patches with jigsaw fractures, point to a cohesive lahar deposit that was generated from a debris avalanche.

This unit rests on top of the Ambato basin volcano-sedimentary succession (Fig. 6, 7). Given that the glacially-formed valleys channelized this debris avalanche, we suggest that the age of the DAD-4 is younger than the LGM event.

Huisla-Mulmul tephra fallout deposits. One of the main features of the Ambato basin stratigraphic succession is the presence of 4 major tephra fallout deposits (here named as TFD-1 to -4), which are interlayered with the debris avalanche and block-and-ash-flow deposits from Carihuairazo volcano (Fig. 6, 7). The isopach maps presented by Ordóñez (2012) show thickness decreasing from the SE towards the NW of the Ambato basin (Fig. 9, 10), pointing to the Huisla-Mulmul volcanic complex as the potential source. This interpretation is supported by geochemical data (Fig. 11) of the juvenile pumice fragments from these deposits that define a regular trend with the lavas sampled in these edifices (see below). We summarize below the main characteristics of these deposits.

Tephra fallout deposit 1 (TFD-1). This layer crops out in the entire Ambato basin, with thickness from 3-5 m at Totoras, close to Huisla volcano, to less than 1 m at Ambato-Izamba and Chibuleo cross-sections (Fig. 9). This deposit is composed of white, highly vesiculated, crystal-poor (< 5 vol.%) pumice fragments (80-85 vol.%) of biotite-bearing rhyolitic composition (73-77 wt.% SiO_2), and distinctive metamorphic (mostly greenschist) lithic fragments (10-15 vol.%) belonging to the Alao-Paute Formation of the Eastern Cordillera basement (Aspden and Litherland, 1992). A minor component (~5 vol.%) corresponds to reddish-grey, dense andesitic lithics. At proximal zones (*i.e.*, Totoras; Fig. 3), this unit is well stratified, allowing to identify four different subunits with transitional contacts, defined by grain size, lithic contents, lamination and gradation (Fig. 10a). This unit represents one of the main tephrochronological markers for this part of the Inter Andean valley. Based on 16 thickness measurements and using the formulation of Pyle (1989), Ordóñez (2012) estimated a minimum volume of 1.2 km^3 corresponding to an eruption with a Volcanic Explosive Index (VEI) of 5.

Figure 9. Isopach maps for the tephra fallout deposits of the Ambato basin (modified from Ordóñez, 2012). We stress that no enough data could be gathered to draw an isopach map for TFD-2.

Tephra fallout deposit 2 (TFD-2). This layer crops out in the eastern part of the Ambato basin, between Totoras (1.5 m-thick) and Ambato-Izamba (0.5-0.15 m-thick; Fig. 9). It comprises white, moderately vesiculated pumice fragments (up to 90-95 vol.%) of rhyolitic composition (72-73 wt.% SiO_2), with crystals (5-10 vol.%) of plagioclase, biotite, amphibole, and minor amounts of pyroxenes and magnetite. Additionally, some (5-10 vol.%) hydrothermally-altered lithics, and andesitic fragments were also observed at the unit's base. The base of this deposit is made of a centimetric thick coarse ash layer grading to the main tephra deposit, which shows a normal gradation at the base and a reverse gradation at the top. This layer is interpreted as a pyroclastic surge deposit (Fig. 10c-d) that overlies the previously described 20-30 cm-thick paleosoil. The surge layer includes some small charred twigs (Fig. 10c-d), which were dated twice by radiocarbon at 39 ± 0.4 ka and >45 ka (Table 3). Because of the scarcity of outcrops, we cannot elaborate an isopach map for the TFD-2.

Figure 10. Stratigraphic relationships between DAD and TFD. **(a)** TFD-1 overlying DAD-1 at Coco-Cola cross-section (point 9 in Fig. 6). BF – bloc facies, MF – matrix facies. **(b)** TFD-3 and 4 and the A-TFD at Palahua cross-section (point 7 in Fig. 5). **(c)** TFD-2 and DAD-3 in El Carmen outcrop (point 3 in Fig. 6). Note the paleosoil at the base of the TFD-2 and at the top of a reworked U-BAFD horizon. **(d)** Close-up of El Carmen outcrop. **(e)** DAD-4 overlaid by the distal andesitic tephra fallout deposits, whose origin is probably Chimborazo volcano. Note the presence of the "bicolour layer". **(f)** Distal andesitic tephra fallout deposits at Tisaleo – J.B. Vela road.

Tephra fallout deposit 3 (TFD-3). This layer crops out in the entire Ambato basin, with thickness from 1.2 m at Totoras, to less than 0.2 m at its north-western border. This deposit comprises white, moderately vesiculated, crystal-rich (25-30 vol.%) pumice fragments of high-silica dacitic composition (68-70 wt.% SiO_2). It contains phenocrysts of plagioclase, biotite, amphibole, pyroxenes and magnetite. Some pumice fragments display roughly banded textures between two end-members of light grey and white colours. We note that no chemical heterogeneity has been identified pointing to textural, instead of chemical, differences between both end-members. The deposit is homogeneous, without lamination, excepting the several centimetres thick, coarse ash layers found at the base and top of the unit. Ordóñez (2012) estimated a minimum volume of 0.2 km^3 (based on 20 thickness measurements) that corresponds to an eruption with a volcanic explosive index (VEI) of 4.

Figure 11. Selected major and trace elements *versus* silica content for proximal eruptive products of Carihuairazo volcano as well as the distal deposits of the Ambato basin. We show also for comparison purposes the eruptive products of the neighbouring Puñalica (Narváez et al., 2018) and Huisla-Mulmul (Ancellin et al., 2017) volcanic centres.

Tephra fallout deposit 4 (TFD-4). The TFD-4 crops out in the entire Ambato basin (Fig. 9), although its thickness are lower than the previous tephra fallout deposits, ranging from 0.5 m on the lower Huisla flank, to 0.15-0.2 m in Ambato. This deposit comprises three subunits. The lower one is a homogenous, fine-medium sized, ash fallout deposit with a normal grading. This layer evolves upwards to a well-laminated, ash-rich horizon. Then, the upper layer, which is the thickest and has a wide geographical distribution, is composed of pumice-rich lapilli and coarse ash with a normal gradation. All three layers contain similar crystal-rich (15-25 vol%) white-beige pumice fragments with a mineral assemblage composed of plagioclase, amphibole, biotite, pyroxenes, and Fe-Ti oxides, and dense lithic fragments of grey and reddish-grey andesites. Ordóñez (2012) estimated a minimum volume of 0.1 km^3 for this deposit (21 thickness measurements), leading to a VEI of 4.

Other undifferentiated tephra fallout deposit (U-TFD). Above the TFD-4 deposit, we observe a succession of at least eight tephra fallout deposits that are interlayered with beige-brown, weathered, partially indurated and reworked ash layers (i.e. Cangahua). The overall thickness is of 2-3 m, and individual thicknesses are of about 10-40 cm at the Totoras outcrop. These lapilli-rich layers show a decrease in the grain size and thickness from north to south. They are composed of grey to dark brown, andesitic scoria fragments, grading from coarse scoria to lapilli (up to 5 cm in diameter). We are unable to draw individual isopach maps for these deposits, however, based on the grain size and some scarce geochemical data (not shown), we propose the Huisla-Mulmul volcanic complex as their source. This sequence is covered by the DAD-4 (Fig. 5f, 10b).

Distal andesitic tephra fallout deposits (A-TFD). At least eight tephra fallout deposits crop out in the western part of the Ambato basin, between Mocha, Tisaleo and J.B. Vela towns (Fig. 3). These tephra fallout deposits are composed of dense, dark-brown, andesitic (56.5-58.5 wt.% SiO_2) scoria with minor amounts of dense, lithic fragments. These deposits are interlayered with reworked ash layers with disseminated scoria fragments and often transitional contacts between tephra and ash horizons. The total succession is 7-8 m thick, with individual scoria layers ranging from 5 to 50 cm in the Mocha – J.B. Vela road (Fig. 10f). The thickness of these layers regionally decreases toward the north-east of the Ambato basin, whereas these layers are absent to the west, above 3400-3600 m. Although a detailed study of these layers is beyond the scope of this study, geochemical data from scoria fragments suggest that these tephra layers have been emitted by the nearby Chimborazo volcano (Fig. 12, see below). In the middle-lower part of this succession, we observed a key horizon consisting of two fallout layers of almost similar thickness (between 10 and 15 cm thick). The lower one consists of dark grey-brown scoria with scarce altered lithics (2 cm maximum) and the upper one consists of light grey-beige scoria (4 cm maximum) with scarce non-altered, andesitic lithics. We interpret this double layer as corresponding to the Chimborazo volcano key horizon "III" (Samaniego et al., 2012). Given that this horizon covers glacial deposits interpreted as formed during the Last Glacial Maximum, we propose an age younger than 20-30 ka. This tephra succession, including the bicolour layer, covers the DAD-4 (Fig. 10e-f).

The Puñalica volcano. This lava-dominated cone is composed of a succession of lava flows that are unaffected by glacial erosion. These lavas extend up to 10-11 km towards the north-east, up to the Río Mocha valley and Cevallos town (Fig. 3). These lavas cover the succession of distal andesitic tephra fallout deposits (A-TFD, Fig. 10f). Puñalica lavas are mostly basaltic andesites and andesites (55-60 wt.% SiO_2) with a mineral assemblage composed of plagioclase, ortho- and clino-pyroxene, and frequent olivine phenocrysts. Some of these samples were described by Narvaez et al. (2018).

The upper part of Puñalica is composed of proximal lava flows and pyroclastic fallout deposits (54-56 wt.% SiO_2) cropping out on its upper south-east flank. These deposits correspond to lithic-rich centimetric-to-decimetric size layers covering the youngest lava flows. At the southern part of the cone, in the Quebrada Olalla valley (Fig. 3), these deposits represent a succession of several 10 to 50 cm-thick layers composed of juvenile scoria bombs and dense prismatically-jointed blocks (up to 30 cm in diameter) of andesitic composition (54-58 wt.% SiO_2). Field relationships of the

Puñalica lavas and moraine deposits in the Río Pachanlica valley to the south of the cone allowed Clapperton (1990) to postulate that the activity of this cone occurred between 18 and 14 ka. This assumption was corroborated by a K-Ar age obtained from a distal lava sample of Puñalica that yielded an age of 18 ± 3 ka (RIO18; Bablon et al., 2019). This datation supports a pre-Holocene age for the oldest Puñalica lavas.

The 1698 CE debris flow deposit. The youngest deposit cropping out in the quebradas draining the Carihuairazo massif (*i.e.*, Chiquicahua, Pataló, Quichibí, Terremoto, Catequilla and Pachanlica-Olalla-Mocha; Fig. 3) is a 2-4 m-thick, dark, matrix-rich deposit composed by fine sand and silt materials, with some scarce 10-40 cm rounded blocks (Vásconez et al., 2009; Vasconez et al., 2019). One of the most conspicuous characteristics of this deposit is the presence of subvertical prismation, which were interpreted as desiccation cracks implying that this deposit was water-saturated. This deposit forms flat terraces on the valley floor and in the medial to distal zones (Ambato basin; Fig. 2c), and covers the reworked distal ash deposits associated with the Tungurahua volcano eruptions from the last millennium (Le Pennec et al., 2008). This deposit originated from small size (1-2 m) landslides affecting the andosol on the upper Carihuairazo flanks as a result of a large earthquake that affected the Ecuadorian Andes on June 20th 1698 (MSK intensity X, M_I of 7.3; Beauval et al., 2010; Wolf, 1904). The landslide's scars are still visible in the topography in the upper flanks of Carihuairazo (black dotted line, Fig. 2d). Based on detailed field mapping (Vásconez et al., 2009) and modelling (Vasconez et al., 2019), these authors estimated a total volume of 80-90 x 10^6 m^3 for these deposits, as well as a total thickness of up to 40 m from the valley bottom at the Rio Ambato. These mudflows destroyed the former Ambato town (Wolf, 1904; Vásconez et al., 2009).

5. Geochemical characteristics as a tool for discriminating the origin of the Ambato basin tephra fallout deposits

Carihuairazo samples define an andesitic to dacitic, medium-K calc-alkaline trend (Fig. 11) ranging from 59 to 66 wt.% SiO_2, with very few samples falling in the field of basaltic andesites (55-56 wt.% SiO_2). No significant chemical and mineralogical differences have been observed between the different volcanic units of Carihuairazo. We note that distal Ambato basin deposits (*i.e.,* debris avalanche and block-and-ash-flow deposits) display the same geochemical compositions as the proximal lava flows and domes. In addition, the mineral assemblage of the proximal and distal units remains unchanged during magmatic differentiation, with a mineral assemblage of plagioclase, ortho- and clino-pyroxene, amphibole, and Fe-Ti oxides.

In contrast, the Ambato basin tephra fallout deposits (red triangles, Fig. 11) display high-silica dacitic to rhyolitic compositions (from 68 to 79 wt.% SiO_2) that clearly define a magmatic trend different than the Carihuairazo one, characterized by higher K_2O and other incompatible elements (such as Rb, Ba, La, Nb, Th; Fig. 11). It is also interesting to note that the silica contents decrease from TFD-1 to TFD-3/4. We also note that these dacitic to rhyolitic compositions lie along the prolongation of the Huisla-Mulmul magmatic trend (yellow triangles, Fig. 11). This information, together with the isopach distribution described previously, argue in favour of the hypothesis that the source of these Plinian events is the Huisla-Mulmul volcanic complex.

In contrast, identifying the source for the younger andesitic tephra samples (A-TFD) is a challenging task. In Fig. 12, we compare the A-TFD samples with those of Chimborazo volcano (Samaniego et al., 2012), including the variation fields for the volcanic products of the volcanoes around the Ambato basin (*i.e.*, Carihuairazo, Puñalica, and Huisla-Mulmul). This comparison highlights that the A-TFD display a rather large geochemical variability similar to that observed for the Chimborazo tephra samples. This supports the hypothesis that the A-TFD are originated from the Chimborazo volcano.

Finally, we also note that Puñalica samples (black stars, Fig. 11) define a homogenous group of magnesium-rich basaltic andesites and andesites (54-60 wt.% SiO_2), with a mineral assemblage composed by plagioclase, ortho- and clino-pyroxene, olivine and Fe-Ti oxides. We stress that olivine is frequent in these lavas, whereas amphibole is absent. When considering at some major elements Harker diagrams (for instance K_2O and MgO *vs.* SiO_2, Fig. 11), Puñalica samples seem to define a single magmatic trend with Carihuairazo. However, some trace elements concentrations (*e.g.*, La, Th) and ratios (*e.g.* Th/La) clearly point to a more complex scenario. This observation argues against a single magmatic system feeding both Carihuairazo and Puñalica volcanoes. Contrasted ages of Carihuairazo (Middle Pleistocene, 220-150 ka) and Puñalica (< 18 ka) volcanoes also support this assumption.

Figure 12. Comparison between the regional andesitic tephras (A-TFD) and the Chimborazo tephras (white dots and thin black line field, Samaniego et al., 2012). We also show the variation fields for

Carihuairazo (this work), Puñalica (Narváez et al., 2018) and Huisla-Mulmul (both proximal lavas and tephras, Ancellin et al., 2017) volcanoes.

6. Discussion

6.1. The evolution of Carihuairazo volcano with recurrent sector collapses

The oldest volcanic units identified in the region correspond to two domes located to the south of the Rio Ambato valley (*cf.* Sunatza and Cruz Maqui domes), dated by Bablon et al. (2019) at 512 ± 9 ka (Fig. 13b). This age is almost contemporaneous to those obtained for Huisla volcano (490-620 ka; Bablon et al., 2019) and corresponds to the oldest Carihuairazo volcanic unit. The main volcanic succession of the Carihuairazo cone itself correspond to thick lava flows that form its outer western and southern flanks. Lava flows samples from the lower flanks yield ages in the range of 200-230 ka (Samaniego et al., 2012). This Basal lava flow succession represents the main cone-building stage of Carihuairazo (Fig. 13c), responsible of the construction of an old edifice that was affected by the successive sector collapses. This edifice was capped by a summit dome complex, whose remnants were not identified, but produced the Chibuleo block-and-ash-flow deposits cropping out in the northern lower flank (Fig. 13d). This block-and-ash-flow succession indicates of a large dome-forming phase at Carihuairazo. We were unable to date this volcanic succession, however, given that it is covered by the TFD-1 deposit, we consider that it predates the recurrent volcanic sector collapses and the block-and-ash-flow deposits that affected Carihuairazo later.

The old Carihuairazo edifice suffered a large sector collapse that formed some “torevas” in the proximal north-western part of the avalanche scar, and whose remnants correspond to the Milincocha hills. This sector collapse triggered a large debris avalanche deposit (DAD-1, Fig. 13d) that reached the Ambato basin 20-25 km from the current Carihuairazo summit. This debris avalanche deposit overlies the Chalupas ignimbrite and the older Ambato basin deposits. The DAD-1 is covered by the conspicuous TFD-1. Based on isopach maps and geochemical arguments, this tephra deposit comes from the nearby Huisla-Mulmul volcanic complex, whose younger lavas (from Mulmul edifice) were dated at 140-175 ka by Bablon et al. (2019). After the DAD-1 sector collapse, Carihuairazo initiated a reconstruction period characterized by the extrusion of lava domes responsible for the succession of block-and-ash-flows deposits (L-BAFD). Based on the K-Ar ages of the underlaying Chalupas ignimbrite (216 ± 5 ka; Bablon et al., 2020), and the overlaying L-BAFD (206 ± 4 ka), the age of the DAD-1 is well constrained between these two ages. Following this phase of dome growth and collapse, Carihuairazo reconstructed around 200-185 ka, forming the Intermediate lava flow succession of the north-eastern and the upper western flanks of the volcano (Fig. 13e). This period was also characterised by dome growth and collapse (U-BAFD) and ended with a smaller debris avalanche deposit (DAD-2; Fig. 13e). We argue that this succession of events succeeded in a relatively short time scale due to the lack of erosional discordances throughout most of the Ambato basin stratigraphic succession (Fig. 6).

Figure 13. Synthesis cartoons of the eruptive history of the Ambato Basin since 800 ka. Note that the morphology of the landscape before the construction of volcanoes (basement in grey and ~500 ka old domes in green) are speculative and deduced from the present elevation of the basement around them. Same legend as in Fig. 3.

The upper part of the Carihuairazo cone was constructed around 150-175 ka, when it reached its maximum height, about 4800-5000 m asl. The remnants of this eruptive stage form the Terminal lava succession (Fig. 13f), as well as a few lava domes that crop out along the Pachanlica valley (Santa Rosa, Cahuito, and Pitiunga domes, Fig. 3). As no ages younger than 157 ± 5 ka have been obtained from this volcano, we suggest that Carihuairazo experienced a recurrent sequence of sector collapses and dome growth/collapse events (DAD-1, L-BAFD, DAD-2, and U-BAFD) during about 50 kyr. Thus, the Carihuairazo evolution roughly lasted between 230 and 150 ka.

The upper part of the U-BAFD unit appears as a soil-like, dark horizon, suggesting a repose time of the deposition process. This disconformity is in agreement with two radiocarbon ages (39.0 ± 0.4 ka; >45 ka) obtained at the base of the overlying TFD-2, implying that the forthcoming debris avalanche deposit (DAD-3 and -4, Fig. 13g) are younger than 40-50 ka. These ages imply that the sector collapse associated with the DAD-3 occurred several tens of thousands of years after the last volcanic activity at Carihuairazo. Then, a younger and smaller sector collapse occurred at Carihuairazo, whose debris avalanche deposit (DAD-4) was mostly channelized by the main drainages of the Ambato basin (Fig. 13g). Based on stratigraphic information, this sector collapse probably occurred during or just after the LGM period (*i.e.*, younger than 20-30 ka). Following this debris avalanche deposit (DAD-4), the only volcanic products deposited on the Ambato basin correspond to regional andesitic tephra fallout deposits that were interpreted to originate from the Chimborazo volcano (Samaniego et al., 2012). The youngest volcanic events that affected this region of the Inter Andean valley correspond to the Puñalica volcano growth (Fig. 13h), that included a succession of effusive eruptions responsible for a large lava field that was dated at 18 ± 3 ka (Bablon et al., 2019), as well as explosive deposits associated with the upper Puñalica pyroclastic cone formation. The structural evolution of Puñalica, as well as the detailed description of its eruptive dynamisms and petrology is beyond the scope of this study and it will be detailed in a forthcoming manuscript. Lastly, during historical times (1698 *CE*), Carihuairazo flanks were affected by widespread landslides triggered by a large regional earthquake, these landslides evolved to large debris flows that flowed by the main drainages.

6.2. Successive destabilization of a summit dome complex

In Ecuador, debris avalanche deposits formed as a result of sector collapses have been described at Chimborazo (Bernard et al., 2008; Samaniego et al., 2012); Tungurahua (Hall et al., 1999; Bablon et al., 2018); Cotopaxi (Hall and Mothes, 2008; Vezzoli et al., 2017); Imbabura (Le Pennec et al., 2011; Andrade et al., 2019); Cubilche (Roverato et al., 2018; Navarrete et al., 2021); Pichincha (Robin et al., 2010); Mojanda-Fuya Fuya (Robin et al., 2009); Huisla-Mulmul (Espín et al., 2019); and Sangay (Monzier et al., 1999; Valverde et al., 2021). The Carihuairazo evolution is a unique case-study in the Ecuadorian context because it experienced at least four sector collapses (and the subsequent debris avalanche deposits, DAD-1 to -4) during its life-time. The first two debris avalanche deposits (DAD-1 and -2), were followed by dome collapse block-and-ash flow deposits (L- and U-BAFD). This stratigraphic evidence implies that following the large DAD-1 event, Carihuairazo started a construction/destruction period comprised in a relatively short time scale that lasted for several 10’s kyr. In contrast, the two youngest debris avalanches (DAD-3 and -4) were unrelated to synchronous volcanic activity. They may have been related to hydrothermal alteration of the edifice, seismic activity, and/or gravitational destabilization related with its location in the eastern flank of the Western Cordillera. In addition, the profiles along the thalwegs of the main drainages of the eastern half of the volcano are similar and not showing a large depression (Fig. 4b-d), suggesting that the successive collapses should be filled by the avalanche deposits and the subsequent eruptive products, and may have been eroded by glacier activity. We should also mention that the first three major DAD occurred before the Last Glacial Maximum, whereas the DAD-4 was a younger and smaller event that did not significantly affect the morphology of the volcano.

6.3. Edifice volumes and eruptive rates

Results of the volumes, eruptive and erosion rates are summarized in Table 4. Eruptive rates should be considered with caution. Indeed, they can be underestimated due to the pyroclastic material missing in the volume calculation and a biased elevation model of the basement beneath the volcano; or overestimated due to an incomplete sampling leading to an erroneous determination of the construction period. However, they provide a first-order estimate of the volcanic output rates. Considering that the construction of the Carihuairazo volcano occurred between 223 ± 6 and 157 ± 5 ka (Samaniego et al., 2012; Table 2), and that the volume of emitted products reached 97 ± 53 km^3, we obtain an eruptive rate of 1.5 ± 0.9 km^3/kyr. This rate is similar or somewhat higher to the values estimated for other Ecuadorian volcanoes such as Viejo Cayambe (1.0-1.5 km^3/ka; Samaniego et al., 2005), Guagua Pichincha (0.6-0.8 km^3/ka; Robin et al., 2010), Chimborazo (0.5-0.8 km^3/ka; Samaniego et al., 2012), and old Tungurahua I (0.6-0.8 km^3/ka; Bablon et al., 2018). At the Andean scale, the eruptive rate estimated for Carihuairazo are higher than that of other well-studied volcanoes such as El Misti (0.63 km^3/ka, Thouret et al., 2001) and Puyehue-Cordón Caulle (0.40–0.50 km^3/ka, Singer et al., 2008). The eruptive rate estimated for Carihuairazo is notably higher than that calculated for most of the large, long-lived Andean volcanoes such as Aucanquilcha (0.05-0.16 km^3/ka, Klemetti and Grunder, 2008); Ampato-Sabancaya (0.10-0.12 km^3/ka, Samaniego et al., 2016), Ubinas (0.10-0.20 km^3/ka, Thouret et al., 2005) and Parinacota (0.25-0.30 km^3/ka, Hora et al., 2007). This difference is mostly due to the fact that Carihuairazo growth is surprisingly short (66 ± 6 ka), in comparison with most of the edifices previously mentioned, whose lifespan is much longer (several hundreds of ka). Indeed, Carihuairazo seems to have grown quite continuously, without long repose periods, as is common in many arc volcanoes.

Finally, considering that the quiescence period of the main edifice of the Carihuairazo volcano started at 157 ± 5 ka (Table 2), and the eroded volume defined by the current DEM and the pre-erosion modelled paleo-topography, we obtain a volume of eroded material of 18 ± 5 km^3. We used erosion rate to extrapolate the volume of material eroded during its construction (*i.e.*, between 223 and 157 ka), and obtained 8 ± 2 km^3. Adding the volume dismantled by sector collapses during the construction stage of Carihuairazo (DAD-1 to -4), we obtain a total volume of 30 ± 9 km^3, corresponding to an erosion rate of about 0.1 km^3/ka. This latter is similar to the erosion rate obtained for Ecuadorian volcanoes located in the Cordilleras, and higher than those obtained for volcanoes located within the Inter Andean Valley (Bablon et al., 2020), which are less affected by orographic rainfalls and glacial erosion.

6.4. The Carihuairazo evolution and the link with the nearby Chimborazo

In his pioneering work on glacial and volcanic geomorphology, Clapperton (1990) described Chimborazo and Carihuairazo volcanoes as being part of a same volcanic massif. Indeed, both edifices are just 10 km apart and are located on a NE-SW trend roughly parallel to the large crustal tectonic structure named the Chingual-Cosanga-Pallatanga-Puna fault system (CCPP, Baize et al., 2020). In addition, both volcanic systems share a similar geochemical signature (Samaniego et al., 2012; Ancellin et al., 2017). However, the structural development of each volcano is independent and a temporal gap between Carihuairazo and Chimborazo was suggested by Samaniego et al. (2012). This interpretation is based on field observation at the Abraspungo valley, where the older lavas of Carihuairazo (Piedra Negra succession) underlie the older lavas of Chimborazo (Abraspungo lava succession, Samaniego et al., 2012). The new chronological data presented here confirms this hypothesis because Carihuairazo development is constrained between 230 and 150 ka, whereas Chimborazo lifetime is younger than 100-120 ka.

7. Conclusions

Carihuairazo is a mostly andesitic stratovolcano that overlooks the Ambato basin, a tectonic depression located at the southern termination of the Ecuadorian arc. The basal edifice is mainly composed of an andesitic lava flow succession dated at 230-200 ka, followed by an intermediate lava flow succession (200-185 ka) and a terminal lava flow succession (175-150 ka) that included a summit dome complex. This edifice suffered a first sector collapse that was responsible for a large debris avalanche deposit (DAD-1) that covers the entire Ambato basin. This event occurred between 206 ± 4 and 216 ± 5 ka. Then, Carihuairazo started a succession of construction (Intermediate and Terminal lava flow successions) and destruction (L-BAFD, DAD-2, U-BAFD) stages lasting about 50 ky (*i.e.*, from 200 to 150 ka). This volcanic succession is recorded in the Ambato basin, interlayered with several tephra fallout deposits (TFD-1 to -4) whose source is the nearby Huisla-Mulmul volcanic complex. The current morphology of Carihuairazo results from two additional sector collapses (DAD-3 and -4) that occurred during the past 40-50 ka, *i.e.*, following a long period (at least 100 ka) without volcanic activity. The evolution of the Carihuairazo edifice, recorded in the medial-distal deposits of the Ambato basin, represents a unique example in the Ecuadorian arc of an edifice that experienced recurrent sector collapses during a major part of its volcanic history.

Acknowledgments

This work is part of an Ecuadorian-French cooperation programme carried out between the Instituto Geofísico, Escuela Politécnica Nacional (IG-EPN) and the Institut de Recherche pour le Développement (IRD, France) through a "Laboratoire Mixte International" program entitled "Séismes et Volcans dans les Andes du Nord". We thank Bastien Eschbach for his help during preparations and K-Ar measurements of some samples. This research was partially financed by the French Government Laboratory of Excellence initiative n◦ ANR-10-LABX-0006, the Région Auvergne and the European Regional Development Fund. This is Laboratory of Excellence ClerVolc contribution number XXX.

References

Ancellin, M.A., Samaniego, P., Vlastélic, I., Nauret, F., Gannoun, A., Hidalgo, S., 2017. Across-arc versus along-arc Sr-Nd-Pb isotope variations in the Ecuadorian volcanic arc. Geochem. Geophys. Geosyst. 18, 1163-1188.

Andrade, S.D., van Wyk de Vries, B., Robin, C., 2019. Imbabura volcano (Ecuador): the influence of dipping-substrata on the structural development of composite volcanoes during strike-slip faulting. J. Volcanol. Geotherm. Res. 385, 68–80.

Araujo, S., Valette, B., Potin, B., Ruiz, M., 2021. A preliminary seismic travel time tomography beneath Ecuador from data of the national network. J. S. Am. Earth Sci. 111, 103486.

Aspden, J.A., Litherland, M., 1992. The geology and Mesozoic collisional history of the Cordillera Real, Ecuador. Tectonophysics 205, 187–204.

Bablon, M., Quidelleur, X., Samaniego, P., Le Pennec, J.L., Lahitte, P., Liorzou, C., Bustillos, J.E., Hidalgo, S., 2018. Eruptive chronology of Tungurahua volcano

(Ecuador) revisited based on new K-Ar ages and geomorphological reconstructions. J. Volcanol. Geotherm. Res. 357, 378–398.

Bablon, M., Quidelleur, X., Samaniego, P., Le Pennec, J.L., Audin, L., Jomard, H., Baize, S., Liorzou, C., Hidalgo, S., Alvarado, A., 2019. Interactions between volcanism and geodynamics in the southern termination of the Ecuadorian arc. Tectonophysics 751, 54-72.

Bablon, M., Quidelleur, X., Siani, G., Samaniego, P., Le Pennec, J.L., Nouet, J., Liorzou, C., Santamaría, S., Hidalgo, S., 2020. Glass shard K-Ar dating of the Chalupas caldera major eruption: Main Pleistocene stratigraphic marker of the Ecuadorian volcanic arc. Quaternary Geochronology 57, 101053.

Baize, S., Audin, L., Alvarado, A., Jomard, H., Bablon, M., Champenois, J., Espin, P., Samaniego, P., Quidelleur, X., Le Pennec, J.L., 2020. Active tectonics and earthquake geology along the Pallatanga fault, Central Andes of Ecuador. Frontiers in Earth Science 8, 193.

Beate, B., Hammersley, L., DePaolo, D., Deino, A.I., 2006. La Edad de la Ignimbrita de Chalupas, prov. de Cotopaxi, Ecuador, y su importancia como marcador estratigráfico. 6th Jornadas en Ciencias de la Tierra (EPN, Quito), pp. 68–71.

Beauval, C., Yepes, H., Bakun, W.H., Egred, J., Alvarado, A., Singaucho, J.C., 2010. Locations and magnitudes of historical earthquakes in the Sierra of Ecuador (1587-1996). Geophysical Journal International 181, 1613–1633.

Belousov, A., Belousova, M., Voight, B., 1999. Multiple edifice failures, debris avalanches and associated eruptions in the Holocene history of Shiveluch volcano, Kamchatka, Russia. Bull. Volcanol. 61, 324–342.

Bernard, B., van Wyk de Vries, B., Barba, B., Robin, C., Leyrit, H., Alcaraz, S., Samaniego, P., 2008. The Chimborazo sector collapse and debris avalanche: deposit characteristics as evidence of emplacement mechanisms. J. Volcanol. Geotherm. Res. 176, 36-43.

Calder, E.S., Lavallée, Y., Kendrick, J.E., Bernstein, M., 2015. Lava dome eruptions. The Encyclopedia of Volcanoes, 2nd ed.; Sigurdsson, H., Houghton, B., McNutt, S., Rymer, H., Stix, J., Eds, 343-362.

Cassignol, C., Gillot, P.Y., 1982. Range and effectiveness of unspiked potassium-argon dating: experimental groundwork and applications, in: Odin, G.S. (Ed.), Numerical Dating in Stratigraphy. John Wiley & Sons, pp. 159–179.

Clapperton, C.M., 1990. Glacial and volcanic geomorphology of the Chimborazo-Carihuairazo Massif, Ecuadorian Andes. Trans. R. Soc. Edinb. Earth Sci. 81, 91–116.

Cotten, J., Le Dez, A., Bau, M., Caroff, M., Maury, R.C., Dulski, P., Fourcade, S., Bohn, M., Brousse, R., 1995. Origin of anomalous rare-earth element and Yttrium enrichments in subaerial exposed basalts: evidence from French Polynesia. Chem. Geol. 119, 115–138.

Dibacto, S., Lahitte, P., Karátson, D., Hencz, M., Szakács, A., Biró, T., Kovács, I., Veres, D., 2020. Growth and erosion rates of the East Carpathians volcanoes constrained by numerical models: Tectonic and climatic implications. Geomorphology 368, 107352.

Espín, P., Mothes, P., Hall, M., Valverde, V., Keen, H., 2019. The "Mera" lahar deposit in the upper Amazon basin: Transformation of a late Pleistocene collapse at Huisla volcano, Central Ecuador. J. Volcanol. Geotherm. Res. 385, 103–119.

Germa, A., Quidelleur, X., Lahitte, P., Labanieh, S., Chauvel, C., 2011. The K–Ar Cassignol–Gillot technique applied to western Martinique lavas: A record of Lesser Antilles arc activity from 2Ma to Mount Pelée volcanism. Quaternary Geochronology 6, 341–355.

Germa, A., Kimball, S., Martens, A., Quidelleur, X., Bablon, M., 2019. Preservation of inherited argon in plagioclase crystals and implication for residence time after reservoir remobilization. In AGU Fall Meeting Abstracts (Vol. 2019, pp. V51F-0120).

Gillot, PY., Hildenbrand, A., Lefèvre, J.C., Albore-Livadie, C., 2006. The K/Ar dating method: principle, analytical techniques, and application to Holocene volcanic eruptions in Southern Italy. Acta Vulcanologica 18, 55–66.

Gillot, P.Y., Cornette, Y., Max, N., Floris, B., 1992. Two reference materials, trachytes MDO- G and ISH-G, for argon dating (K-Ar and 40Ar/39Ar) of Pleistocene and Holocene rocks. Geostand. Newslett. 16, 55–60.

Glicken, H., 1991. Sedimentary architecture of large volcanic-debris avalanches. Sedimentation in Volcanic Settings, SEPM Spec. Pub. 45, 99–106.

Grosse, P., Orihashi, Y., Guzmán, S.R., Sumino, H., Nagao, K., 2018. Eruptive history of Incahuasi, Falso Azufre and El Cóndor Quaternary composite volcanoes, southern Central Andes. Bulletin of Volcanology 80, 44.

Hall, M.L., Robin, C., Beate, B., Mothes, P., Monzier, M., 1999. Tungurahua Volcano, Ecuador: structure, eruptive history and hazards. J. Volcanol. Geotherm. Res. 91, 1–21.

Hall, M.L., Samaniego, P., Le Pennec, J.L., Johnson, J., 2008. Late Pliocene to present volcanism in the Ecuadorian Andes. J. Volcanol. Geotherm. Res. 176, 1-6.

Hall, M.L., Mothes, P., 2008. The rhyolitic–andesitic eruptive history of Cotopaxi volcano, Ecuador. Bull. Volcanol. 70, 675–702.

Harford, C.L., Pringle, M.S., Sparks, R.S.J., Young, S.R., 2002. The volcanic evolution of Montserrat using 40Ar/39Ar geochronology. Geological Society, London, Memoirs 21, 93–113.

Harpel, C.J., de Silva, S., Salas, G., 2011. The 2 Ka Eruption of Misti Volcano, Southern Peru-The Most Recent Plinian Eruption of Arequipa's Iconic Volcano. Geol. Soc. Am. Spec. Pap. 484, 72.

Hess, J.C., Lippolt, H.J., 1994. Compilation of K-Ar Measurements on HD-B1 Standard Bio- tite, 1994 Status Report. Phaneroz. Time Scale, Bull. Liais. Inform. IUGS Subcomm. Geochronol. p. 122.

Hora, J.M., Singer, B.S., Wörner, G., 2007. Volcano evolution and eruptive flux on the thick crust of the Andean Central Volcanic Zone: 40Ar/39Ar constraints from Volcan Parinacota, Chile. Geol. Soc. Am. Bull. 119, 343–362.

Hughes, R.A., Pilatasig, L.F., 2002. Cretaceous and tertiary terrane accretion in the cordillera Occidental of the Andes of Ecuador. Tectonophysics 345, 29–48.

Jaillard, E., Ordóñez, M., Suarez, J., Toro, J., Iza, D., Lugo, W., 2004. Stratigraphy of the late Cretaceous–Paleogene deposits of the Cordillera Occidental of central Ecuador: geodynamic implications. J. S. Am. Earth Sci. 17, 49–58.

Klemetti, E.W., Grunder, A.L., 2008. Volcanic evolution of Volcán Aucanquilcha: a long- lived dacite volcano in the Central Andes of northern Chile. Bull. Volcanol. 70, 633–650.

Lahitte, P., Samper, A., Quidelleur, X., 2012. DEM-based reconstruction of southern Basse-Terre volcanoes (Guadeloupe archipelago, FWI): Contribution to the Lesser Antilles Arc construction rates and magma production. Geomorphology 136, 148–164.

Lahitte, P., Dibacto, S., Karátson, D., Gertisser, R., Veres, D., 2019. Eruptive history of the Late Quaternary Ciomadul (Csomád) volcano, East Carpathians, part I: timing of lava dome activity. Bull. Volcanol. 81, 27.

Lavenu, A., Noblet, C., Bonhomme, M.G., Egüez, A., Dugas, F., Vivier, G., 1992. New K-Ar age dates of Neogene and Quaternary volcanic rocks from the Ecuadorian Andes: Implications for the relationship between sedimentation, volcanism, and tectonics. J. S. Am. Earth Sci. 5, 309–320.

Le Pennec, J.L., Jaya, D., Samaniego, P., Ramón, P., Moreno Yánez, S., Egred, J., van der Plicht, J., 2008. The AD 1300–1700 eruptive periods at Tungurahua volcano, Ecuador, revealed by historical narratives, stratigraphy and radiocarbon dating, J. Volcanol. Geotherm. Res. 176, 70-81.

Le Pennec, J.L., Ruiz, A.G., Eissen, J.P., Hall, M.L., Fornari, M., 2011. Identifying potentially active volcanoes in the Andes: radiometric evidence for late Pleistocene-early Holocene eruptions at Volcán Imbabura, Ecuador. J. Volcanol. Geotherm. Res. 206, 121–135.

Marino, J., Samaniego, P., Manrique, N., Valderrama, P., Roche, O., van Wyk de Vries, B., Guillou, H., Zerathe, S., Arias, C., Liorzou, C., 2021. The Tutupaca volcanic complex (Southern Peru): Eruptive chronology and successive destabilization of a dacitic dome complex. J. S. Am. Earth Sci. 110, 103227.

Monzier, M., Robin, C., Samaniego, P., Hall, M.L., Cotten, J., Mothes, P., Arnaud, N., 1999. Sangay volcano, Ecuador: structural development, present activity and petrology. J. Volcanol. Geotherm. Res. 90, 49-79.

Mook, W.G, van der Plicht, J., 1999. Reporting 14C activities and concentrations. Radiocarbon 41, 227-239.

Narváez, D., Rose-Koga, E., Samaniego, P., Koga, K.T., Hidalgo, S., 2018. Constraining magma sources using primitive olivine-hosted melt inclusions from Puñalica and Sangay volcanoes (Ecuador). Contrib. Mineral. Petrol. 173, 80.

Navarrete, W.F., Le Pennec, J.L., Solano, S., Liorzou, C., Ruiz, G.A., 2021. A first reconstruction of the evolution of Cubilche Volcanic Complex, Imbabura Province, Ecuador. J. Volcanol. Geotherm. Res. 406, 107023.

Ordóñez, J., 2012. Depósitos volcánicos del Pleistoceno Tardío en la cuenca de Ambato: caracterización, distribución y origen. EPN Memoir, Quito, pp. 192.

Pyle, D., 1989. The thickness, volumen and grainsize of tephra fall deposits. Bull. Volcanol. 55, 523-525.

Raczek, I., Stoll, B., Hofmann, A.W., Peter Jochum, K., 2001. High-precision trace element data for the USGS reference materials BCR-1, BCR-2, BHVO-1, BHVO-2, AGV-1, AGV- 2, DTS-1, DTS-2, GSP-1 and GSP-2 by ID-TIMS and MIC-SSMS. Geostand. Newslett. 25, 77–86.

Robin, C., Mossand, P., Camus, G., Cantagrel, J.M., Gourgaud, A., Vincent, P.M., 1987. Eruptive history of the Colima volcanic complex (Mexico). J. Volcanol. Geotherm. Res. 31, 99-113.

Robin, C., Eissen, J.P., Samaniego, P., Martin, H., Hall, M.L., Cotten, J., 2009. Evolution of the late Pleistocene Mojanda Fuya Fuya volcanic complex (Ecuador), by progressive adakitic involvement in mantle magma sources. Bull. Volcanol. 71, 233-258.

Robin, C., Samaniego, P., Le Pennec, J.L., Fornari, M., Mothes, P., van der Plicht, J., 2010. New radiometric and petrological constraints on the evolution of the Pichincha volcanic complex (Ecuador). Bull. Volcanol. 72, 1109-1129.

Roverato, M., Larrea, P., Casado, I., Mulas, M., Béjar, G., Bowman, L., 2018. Characterization of the Cubilche debris avalanche deposit, a controversial case from the northern Andes, Ecuador. J. Volcanol. Geotherm. Res. 360, 22–35.

Samaniego, P., Martin, H., Monzier, M., Robin, C., Fornari, M., Eissen, J.P., Cotten, J., 2005. Temporal evolution of magmatism at Northern Volcanic Zone of the Andes: The geology and petrology of Cayambe volcanic complex (Ecuador). J. Petrol. 46, 2225-2252.

Samaniego, P., Barba, D., Robin, C., Fornari, M., Bernard, B., 2012. Eruptive history of Chimborazo volcano (Ecuador): A large, ice-capped and hazardous compound volcano of the Northern Andes. J. Volcanol. Geotherm. Res. 221-222, 33-51.

Samaniego, P., Valderrama, P., Mariño, J., van Wyk de Vries, B., Roche, O., Manrique, N., Chedeville, C., Fidel, L., Malnati, J., 2015. The historical (218 ± 14 aAP) explosive eruption of Tutupaca volcano (Southern Peru). Bull. Volcanol. 77, 51.

Samaniego, P., Rivera, M., Mariño, Guillou, H., Liorzou, C., Zerathe, S., Delgado, R., Valderrama, P., Scao, V., 2016. The eruptive chronology of the Ampato-Sabancaya volcanic complex (Southern Peru). J. Volcanol. Geotherm. Res. 323, 110-128.

Samper, A., Quidelleur, X., Boudon, G., Le Friant, A., Komorowski, J.C., 2008. Radiometric dating of three large volume flank collapses in the Lesser Antilles Arc. J. Volcanol. Geotherm. Res. 176, 485–492.

Santamaria, S., Quidelleur, X., Hidalgo, S., Samaniego, P., Le Pennec, J.L., Liorzou, C., Lahitte, P., Córdova, M., Espín, P., 2022. Geochronological evolution of the potentially active Iliniza Volcano (Ecuador) based on new K-Ar ages. J. Volcanol. Geotherm. Res. 107489.

Singer, B.S., Jicha, B.R., Harper, M.A., Naranjo, J.A., Lara, L.E., Moreno-Roa, H., 2008. Eruptive history, geochronology, and magmatic evolution of the Puyehue-Cordón Caulle volca- nic complex, Chile. Geol. Soc. Am. Bull. 120, 599–618.

Steiger, R.H., Jäger, E., 1977. Subcommission on geochronology: Convention on the use of decay constants in geo- and cosmochronology. Earth and Planetary Science Letters 36, 359–362.

Thouret, J.C., Finizola, A., Fornari, M., Suni, J., Legeley-Padovani, A., Frechen, M., 2001. Geology of El Misti volcano nearby the city of Arequipa, Peru. Geol. Soc. Am. Bull. 113, 1593–1610.

Thouret, J.C., Rivera, M., Wörner, G., Gerbe, M.C., Finizola, A., Fornari, M., Gonzales, K., 2005. Ubinas: the evolution of the historically most active volcano in southern Peru. Bull. Volcanol. 67, 557–589.

Valverde, V., Mothes, P.A., Beate, B., Bernard, J., 2021. Enormous and far-reaching debris avalanche deposits from Sangay volcano (Ecuador): Multidisciplinary study and modelling the 30 ka sector collapse. J. Volcanol. Geotherm. Res. 411, 107172.

Van Wyk de Vries, B, Davis, T., 2015. Landslides, debris avalanches and volcanic gravitational deformation. The Encyclopedia of Volcanoes, 2nd ed.; Sigurdsson, H., Houghton, B., McNutt, S., Rymer, H., Stix, J., Eds, 665-685.

Vásconez, R., Hall, M., Mothes, P., 2009. Devastadores flujos de lodo disparados en el volcán Carihuayrazo por el terremoto del 20 de Junio de 1698. Revista Politécnica: Monografía de Geología 7, 30(1), 86-105.

Vascones, F.J., Vásconez, R., Mothes, P., 2019. Flujos de lodo del volcán Carihuairazo provocados por el terremoto de Ambato, Ecuador, en 1698 y su reconstrucción numérica con perspectivas a futuro. Revista Geofísica 69, doi.org/10.35424/rgf.v0i69.937

Vezzoli, L., Apuani, T., Corazzato, C., Uttini, A., 2017. Geological and geotechnical characterization of the debris avalanche and pyroclastic deposits of Cotopaxi Volcano (Ecuador). A contribute to instability-related hazard studies. J. Volcanol. Geotherm. Res. 332, 51-70.

Wolf, T., 1904. Crónica de los fenómenos volcánicos y terremotos en El Ecuador, con algunas noticias sobre otros paises de la América Central y Meridional, desde 1533 hasta 1797 (reedited by N. Martínez). Imprenta de la Universidad Central del Ecuador, Quito.

Yepes, H., Audin, L., Alvarado, A., Beauval, C., Aguilar, J., Font, Y., Cotton, F., 2016. A new view for Ecuador's geodynamics: implication in seismogenic source definition and seismic hazard assessment. Tectonics 35, 1249-1279.

Zemeny, A., Procter, J., Németh, K., Zellmer, G.F., Zernack, A.V., Cronin, S.J., 2021. Elucidating stratovolcano construction from volcaniclastic mass-flow deposits: The medial ring-plain of Taranaki Volcano, New Zealand. Sedimentology 68, 2422-2449.

Table 1. Selected geochemical analyses for Carihuairazo samples.

Table 2. Unspiked K-Ar ages for Carihuairazo volcano.

Table 3. Radiocarbon ages for the Ambato basin deposits.

Table 4. Results of volumes, eruptive and erosion rates calculations obtained from the numerical paleo-surfaces and given at 1-sigma accuracy. Raw volume corresponds to the volume calculated from the surface model without taking into account erosion that occurred during the construction. Total volume corresponds to the sum of the raw volume, the volume eroded during the construction, calculated based on the erosion rate since the end of Carihuairazo construction, and the volume of products mobilized during sector collapse events. Volumes of the four DAD calculated using deposit thicknesses were converted to a dense rock equivalent (DRE) volume using a debris avalanche bulk density of 1950 kg/m^3 (Glicken,1991), and assuming a bulk density of 2600 kg/m^3 for the entire edifice. * Samaniego et al. (2012)

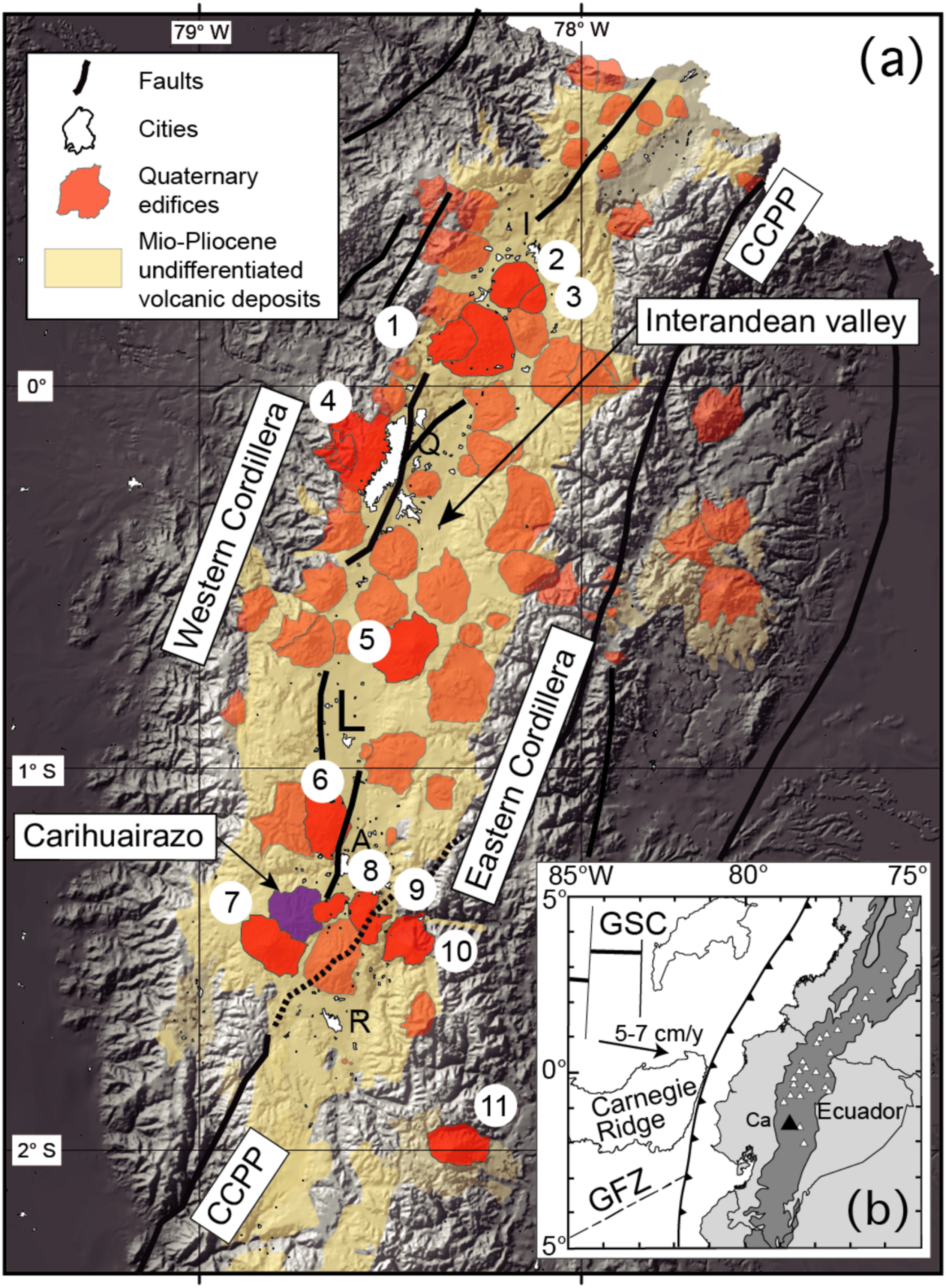
79° W
78° W
(a)
Faults
Cities
Quaternary edifices
Mio-Pliocene undifferentiated volcanic deposits
I
2
3
1
CCPP
Interandean valley
0°
4
Q
Western Cordillera
5
L
Eastern Cordillera
1° S
6
Carihuairazo
A
8
9
7
10
R
11
2° S
CCPP
85°W
80°
75°
5°
GSC
5-7 cm/y
0°
Carnegie Ridge
Ca
Ecuador
GFZ
5°
(b)

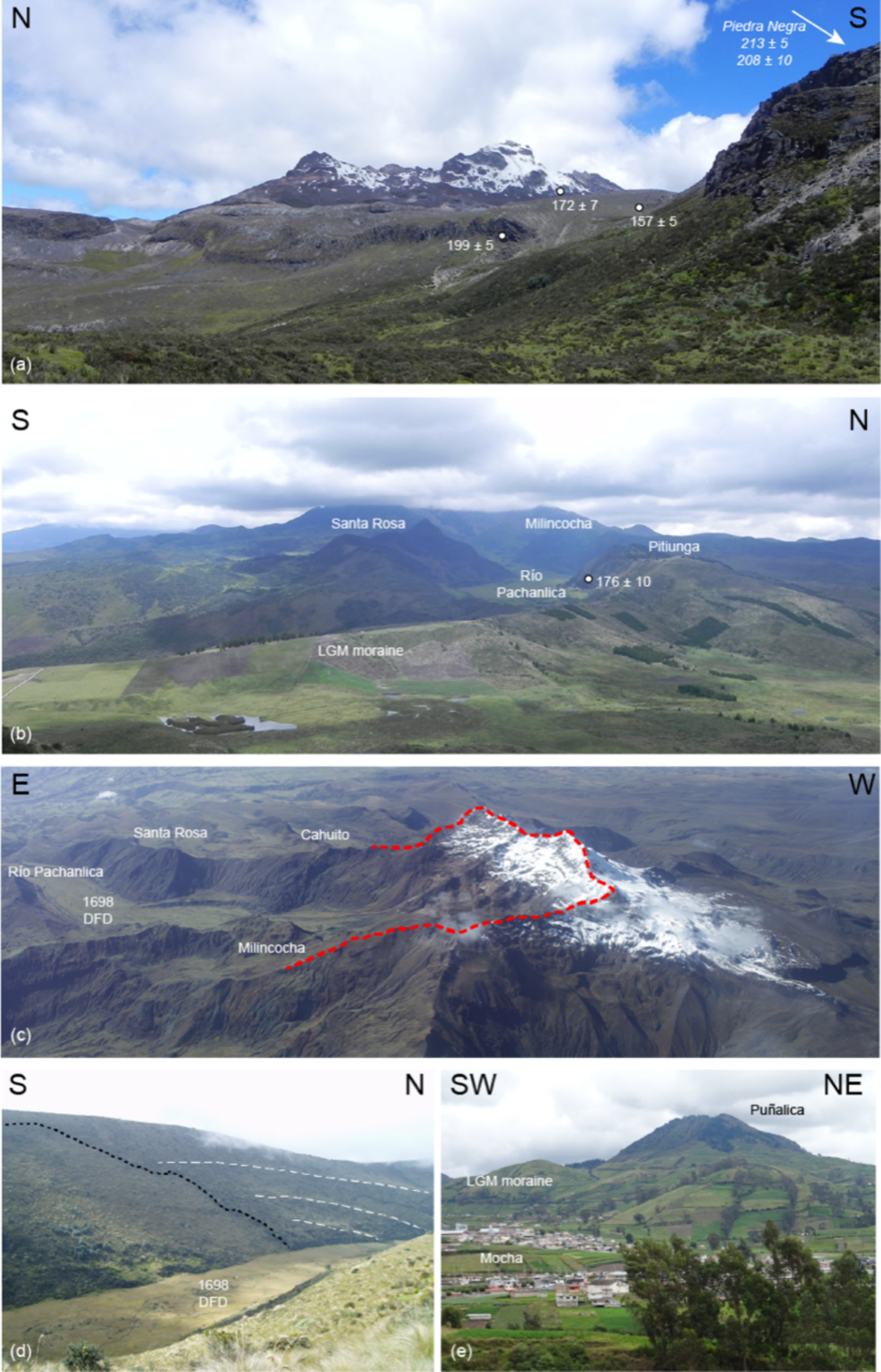
N
S
Piedra Negra
213 ± 5
208 ± 10
172 ± 7
157 ± 5
199 ± 5
(a)
S
N
Santa Rosa
Milincocha
Pitiunga
Río
Pachanlica
176 ± 10
LGM moraine
(b)
E
W
Santa Rosa
Cahuito
Río Pachanlica
1698
DFD
Milincocha
(c)
S
N
1698
DFD
(d)
SW
NE
Puñalica
LGM moraine
Mocha
(e)

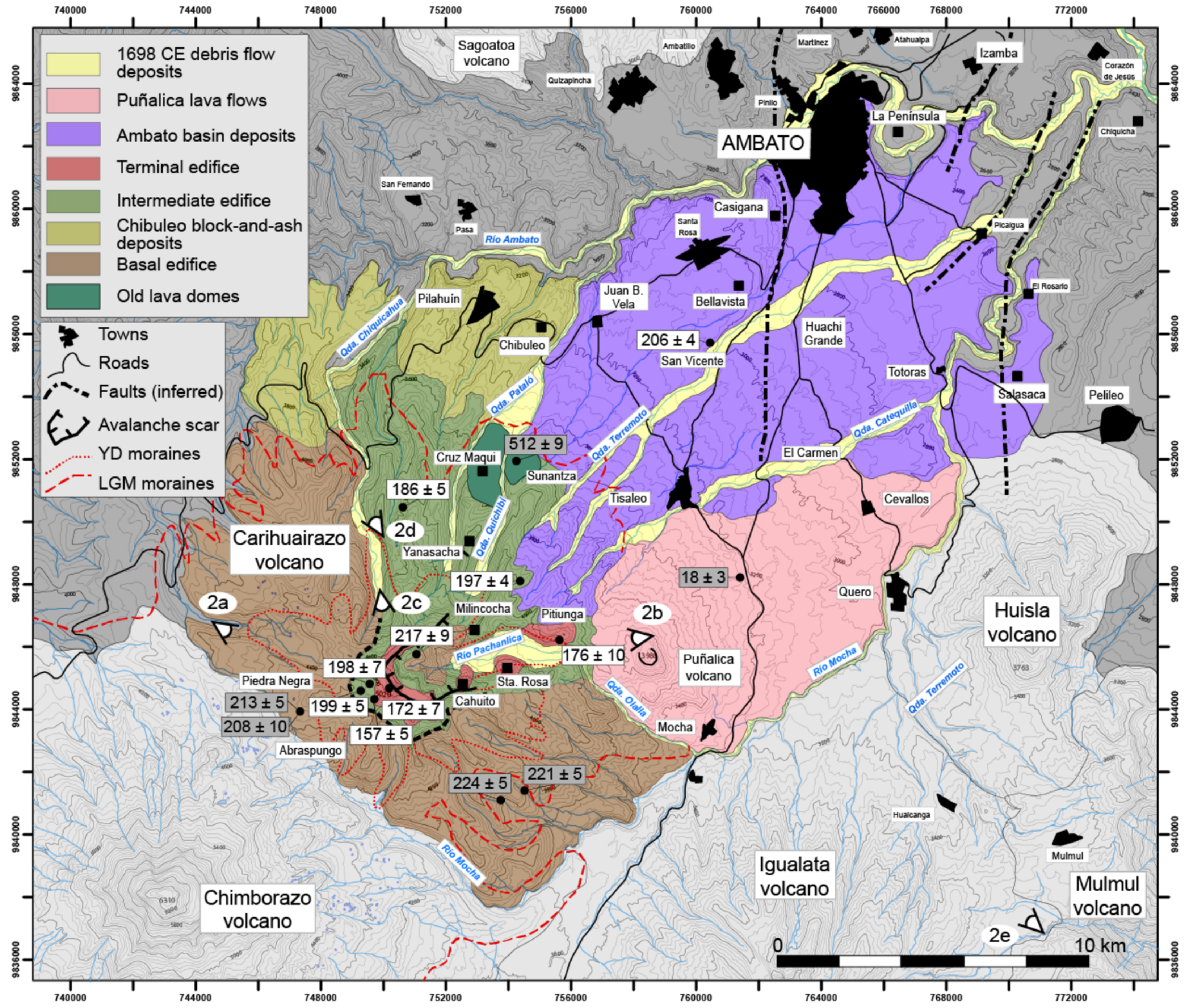
1698 CE debris flow deposits
Puñalica lava flows
Ambato basin deposits
Terminal edifice
Intermediate edifice
Chibuleo block-and-ash deposits
Basal edifice
Old lava domes
Towns
Roads
Faults (inferred)
Avalanche scar
YD moraines
LGM moraines
Sagoatoa volcano
Ambatillo
Martinez
Atahualpa
Izamba
Quizapincha
Pinllo
Corazón de Jesús
La Península
AMBATO
Chiquicha
San Fernando
Pasa
Río Ambato
Casigana
Santa Rosa
Picaigua
El Rosario
Pilahuín
Juan B. Vela
Bellavista
Qda. Chiquicahua
Chibuleo
206 ± 4
San Vicente
Huachi Grande
Totoras
Salasaca
Pelileo
Qda. Pataló
Qda. Terremoto
Qda. Catequilla
512 ± 9
Cruz Maqui
El Carmen
Sunantza
186 ± 5
Tisaleo
Cevallos
2d
Carihuairazo volcano
Yanasacha
Qda. Quichibi
197 ± 4
18 ± 3
Quero
Huisla volcano
2a
2c
Milincocha
Pitiunga
2b
217 ± 9
Río Pachanlica
176 ± 10
Puñalica volcano
198 ± 7
Piedra Negra
Sta. Rosa
Río Mocha
Qda. Terremoto
213 ± 5
199 ± 5
172 ± 7
Cahuito
Qda. Olalla
208 ± 10
157 ± 5
Mocha
Abraspungo
221 ± 5
224 ± 5
Hualcanga
Mulmul
Río Mocha
Chimborazo volcano
Igualata volcano
Mulmul volcano
2e
0
10 km
740000
744000
748000
752000
756000
760000
764000
766000
768000
772000
9864000
9860000
9856000
9852000
9848000
9844000
9840000
9836000

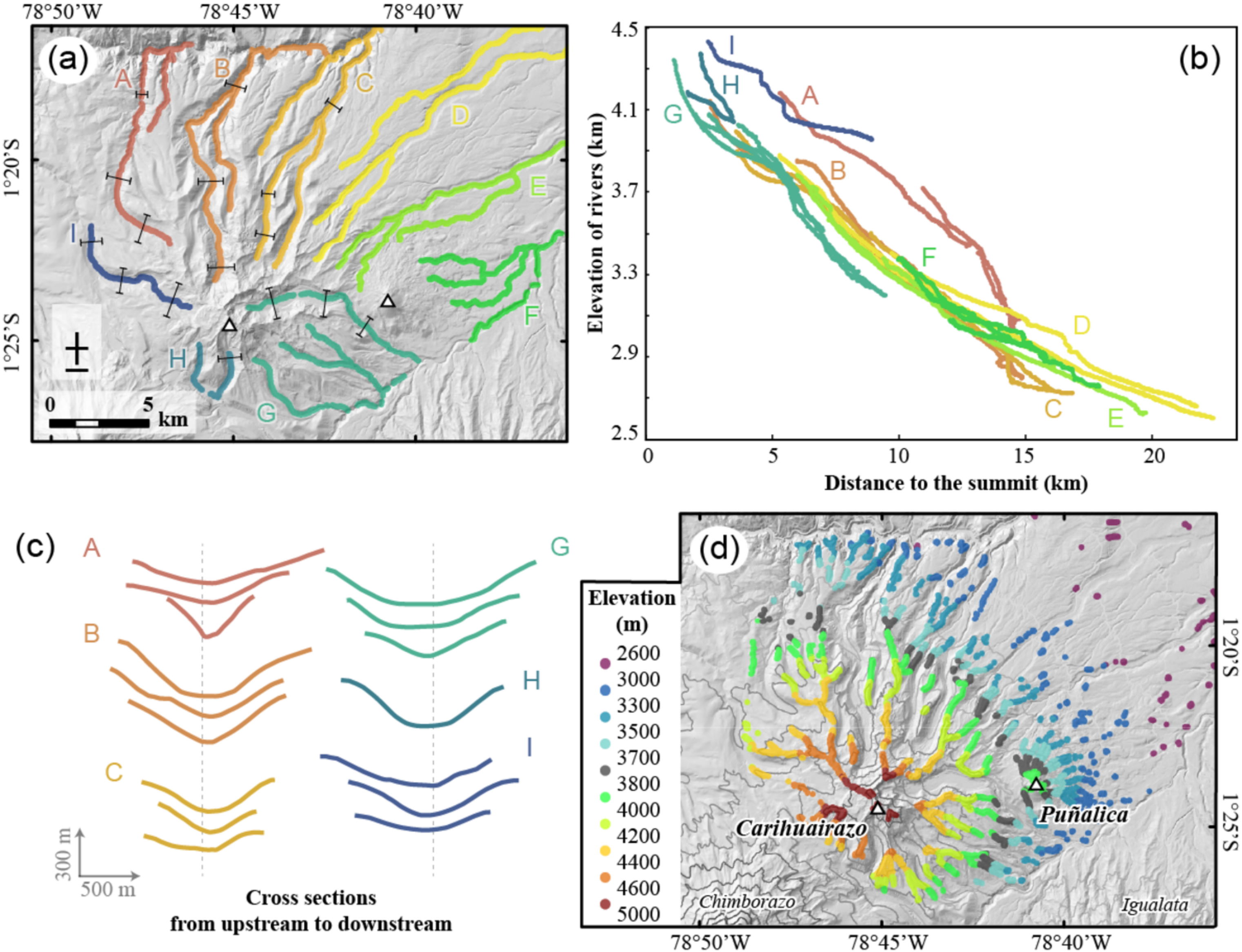
78°50'W
78°45'W
78°40'W
(a)
A
B
C
D
E
F
G
H
I
1°20'S
1°25'S
0
5
km
(b)
4.5
4.1
3.7
3.3
2.9
2.5
Elevation of rivers (km)
0
5
10
15
20
Distance to the summit (km)
I
H
A
G
B
F
D
C
E
(c)
A
B
C
G
H
I
300 m
500 m
Cross sections
from upstream to downstream
(d)
Elevation
(m)
2600
3000
3300
3500
3700
3800
4000
4200
4400
4600
5000
Carihuairazo
Puñalica
Chimborazo
Igualata
1°20'S
1°25'S
78°50'W
78°45'W
78°40'W

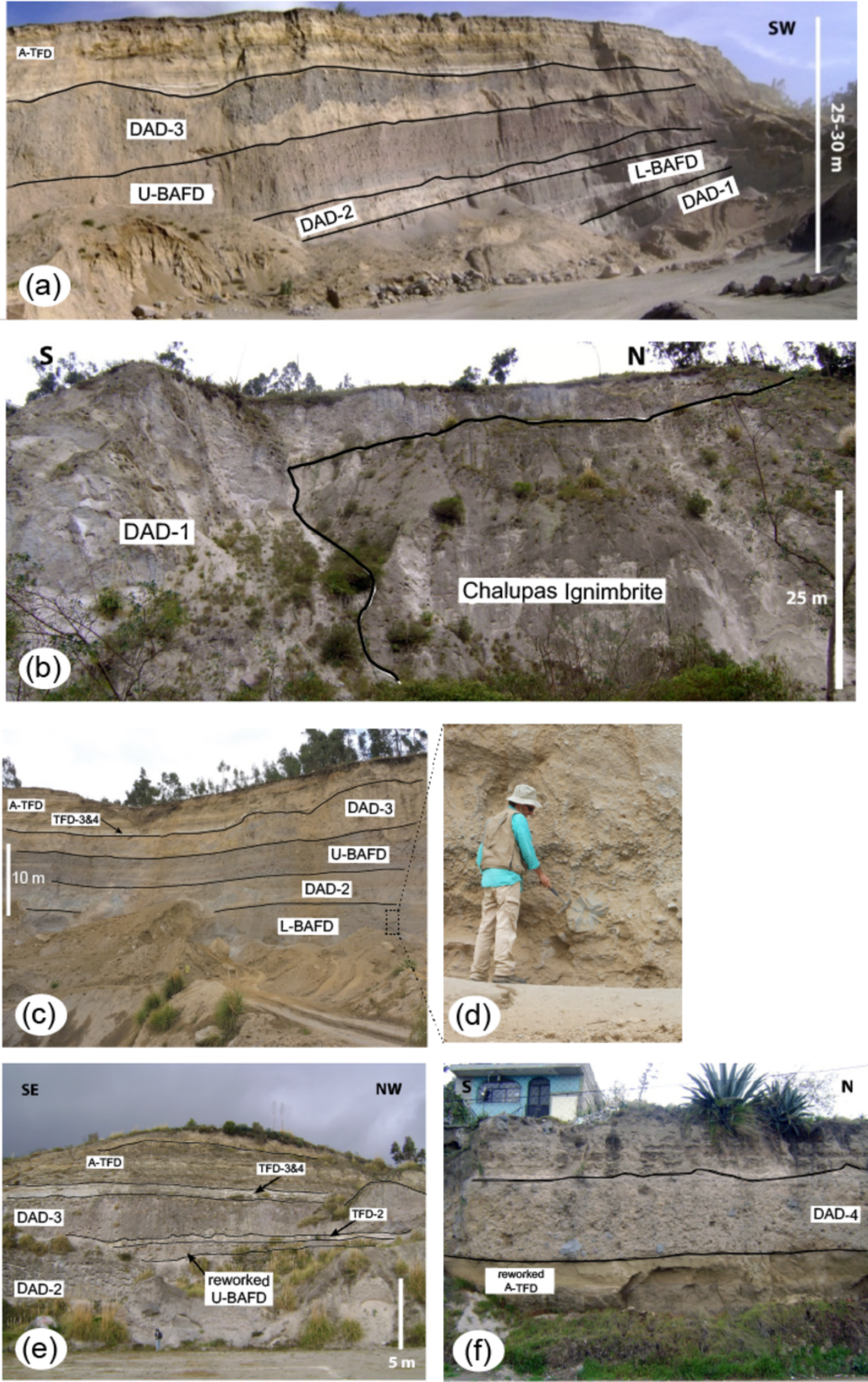
A-TFD
SW
DAD-3
25-30 m
U-BAFD
L-BAFD
DAD-2
DAD-1
(a)
S
N
DAD-1
Chalupas Ignimbrite
25 m
(b)
A-TFD
TFD-3&4
DAD-3
10 m
U-BAFD
DAD-2
L-BAFD
(c)
(d)
SE
NW
A-TFD
TFD-3&4
DAD-3
TFD-2
reworked U-BAFD
DAD-2
(e)
5 m
S
N
DAD-4
reworked A-TFD
(f)

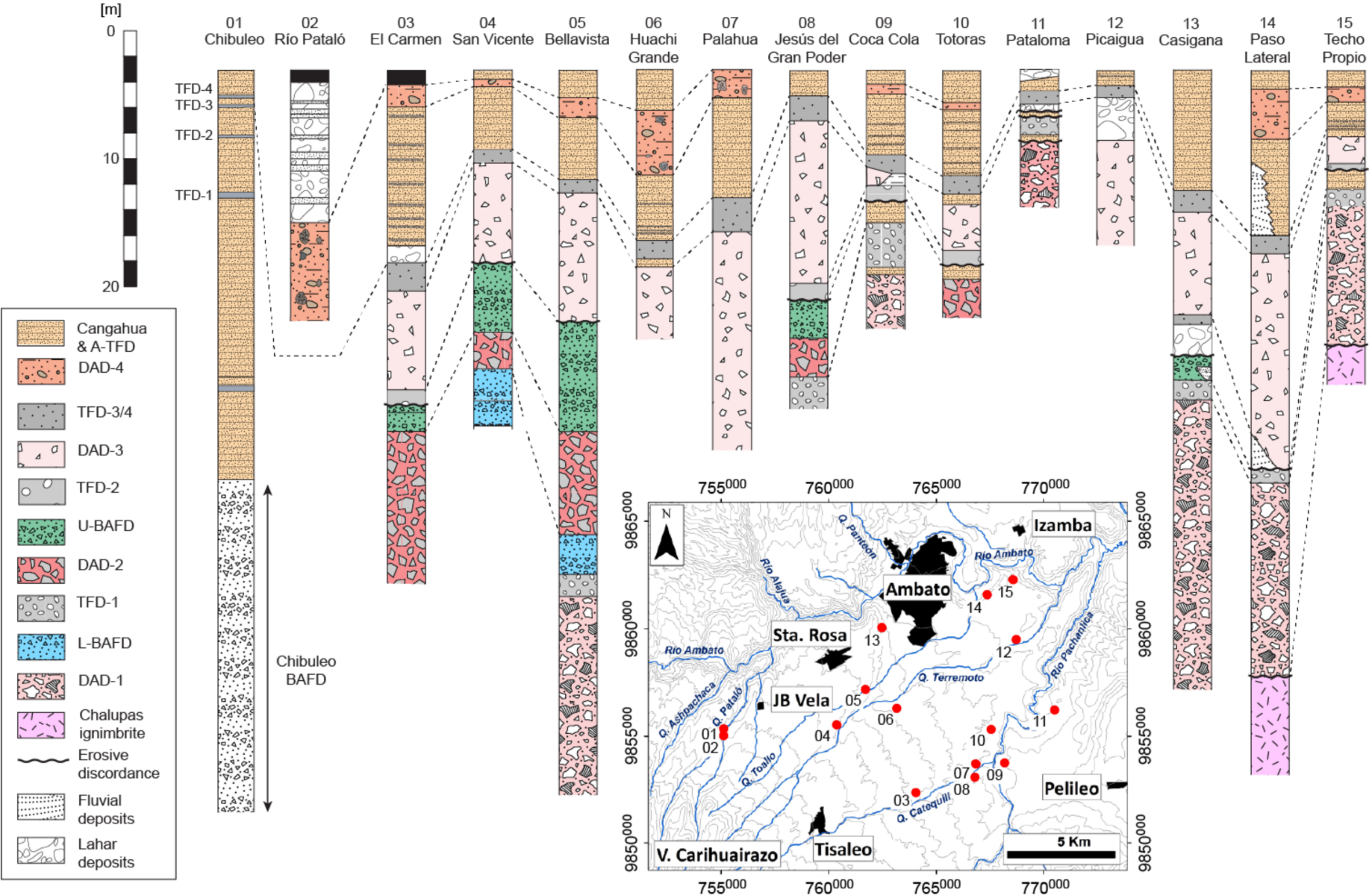
[m]
0
10
20
01 Chibuleo
02 Río Pataló
03 El Carmen
04 San Vicente
05 Bellavista
06 Huachi Grande
07 Palahua
08 Jesús del Gran Poder
09 Coca Cola
10 Totoras
11 Pataloma
12 Picaigua
13 Casigana
14 Paso Lateral
15 Techo Propio
TFD-4
TFD-3
TFD-2
TFD-1
Chibuleo BAFD
Cangahua & A-TFD
DAD-4
TFD-3/4
DAD-3
TFD-2
U-BAFD
DAD-2
TFD-1
L-BAFD
DAD-1
Chalupas ignimbrite
Erosive discordance
Fluvial deposits
Lahar deposits
755000
760000
765000
770000
9865000
9860000
9855000
9850000
N
Izamba
Ambato
Sta. Rosa
JB Vela
Pelileo
Tisaleo
V. Carihuairazo
Q. Pantoon
Río Alajua
Río Ambato
Río Ambato
Río Pachanlica
Q. Terremoto
Q. Ashpachaca
Q. Pataló
Q. Toallo
Q. Catequilla
5 Km
01
02
03
04
05
06
07
08
09
10
11
12
13
14
15

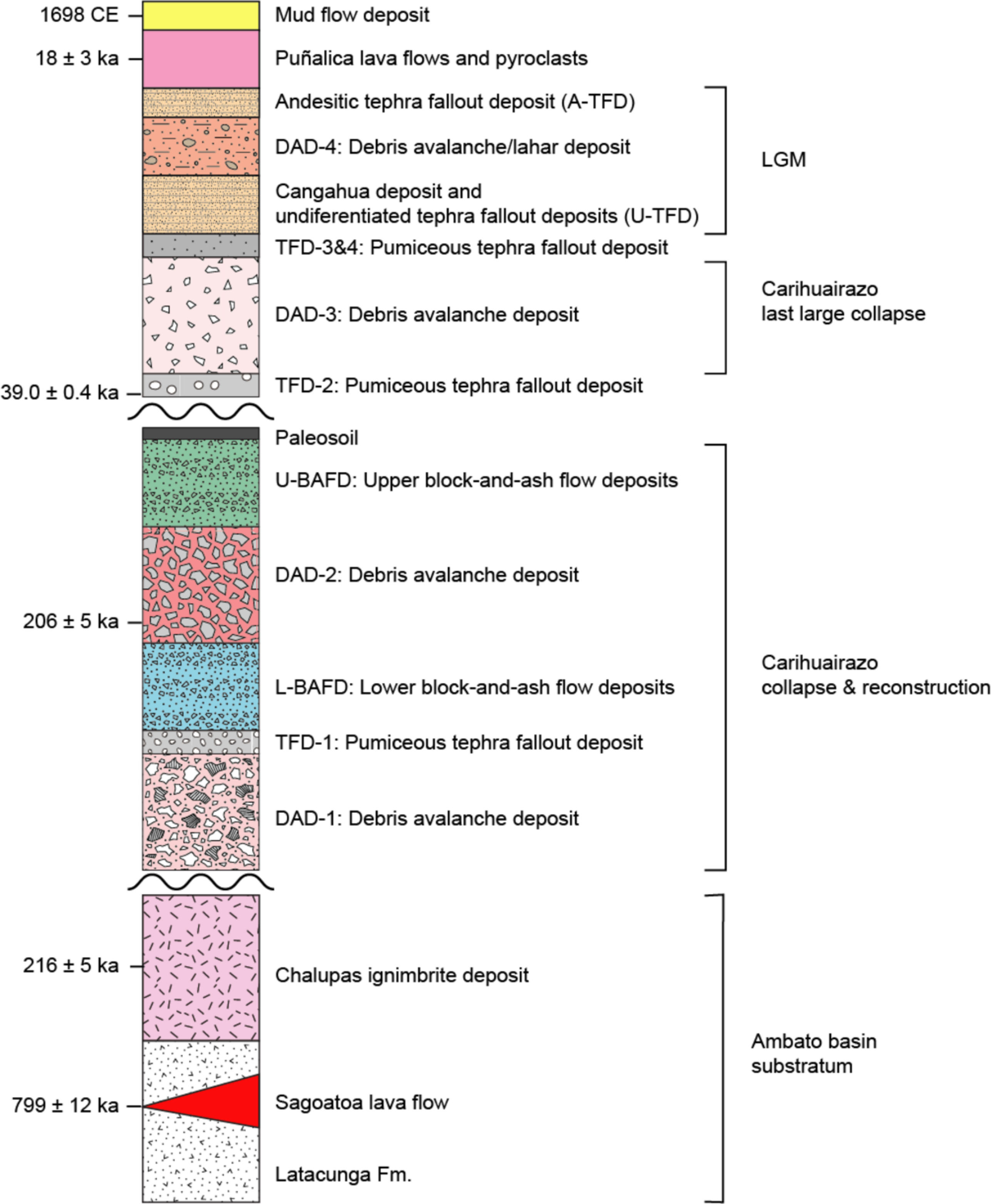
1698 CE
Mud flow deposit
18 ± 3 ka
Puñalica lava flows and pyroclasts
Andesitic tephra fallout deposit (A-TFD)
DAD-4: Debris avalanche/lahar deposit
Cangahua deposit and undiferentiated tephra fallout deposits (U-TFD)
LGM
TFD-3&4: Pumiceous tephra fallout deposit
DAD-3: Debris avalanche deposit
Carihuairazo last large collapse
39.0 ± 0.4 ka
TFD-2: Pumiceous tephra fallout deposit
Paleosoil
U-BAFD: Upper block-and-ash flow deposits
DAD-2: Debris avalanche deposit
206 ± 5 ka
L-BAFD: Lower block-and-ash flow deposits
Carihuairazo collapse & reconstruction
TFD-1: Pumiceous tephra fallout deposit
DAD-1: Debris avalanche deposit
216 ± 5 ka
Chalupas ignimbrite deposit
Ambato basin substratum
799 ± 12 ka
Sagoatoa lava flow
Latacunga Fm.

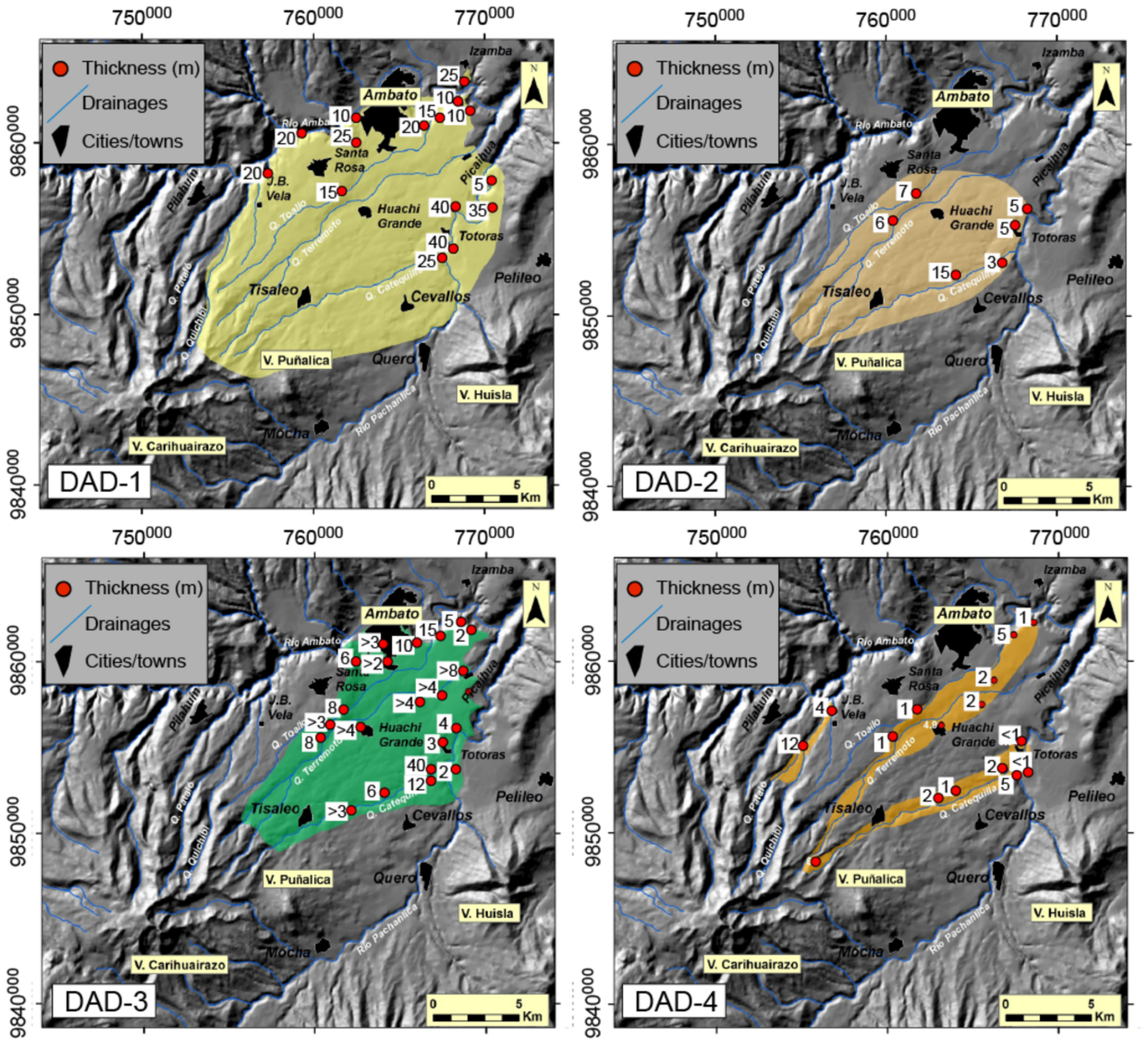
750000
760000
770000
9860000
9850000
9840000
Thickness (m)
Drainages
Cities/towns
DAD-1
DAD-2
DAD-3
DAD-4
Ambato
Izamba
Río Ambato
Santa Rosa
J.B. Vela
Pilahuín
Q. Toallo
Q. Terremoto
Q. Catequilla
Q. Pataló
Q. Quichibí
Huachi Grande
Picaihua
Totoras
Tisaleo
Cevallos
Pelileo
Quero
Mocha
Río Pachanlica
V. Puñalica
V. Huisla
V. Carihuairazo
N
0
5
Km
25
10
15
10
20
20
25
10
20
15
5
40
35
40
25
7
6
5
5
3
15
>3
10
15
5
2
6
>2
>8
>4
>4
8
>3
>4
4
8
3
40
2
12
6
>3
1
5
2
2
4
1
12
1
4.8
<1
2
<1
5
2
1

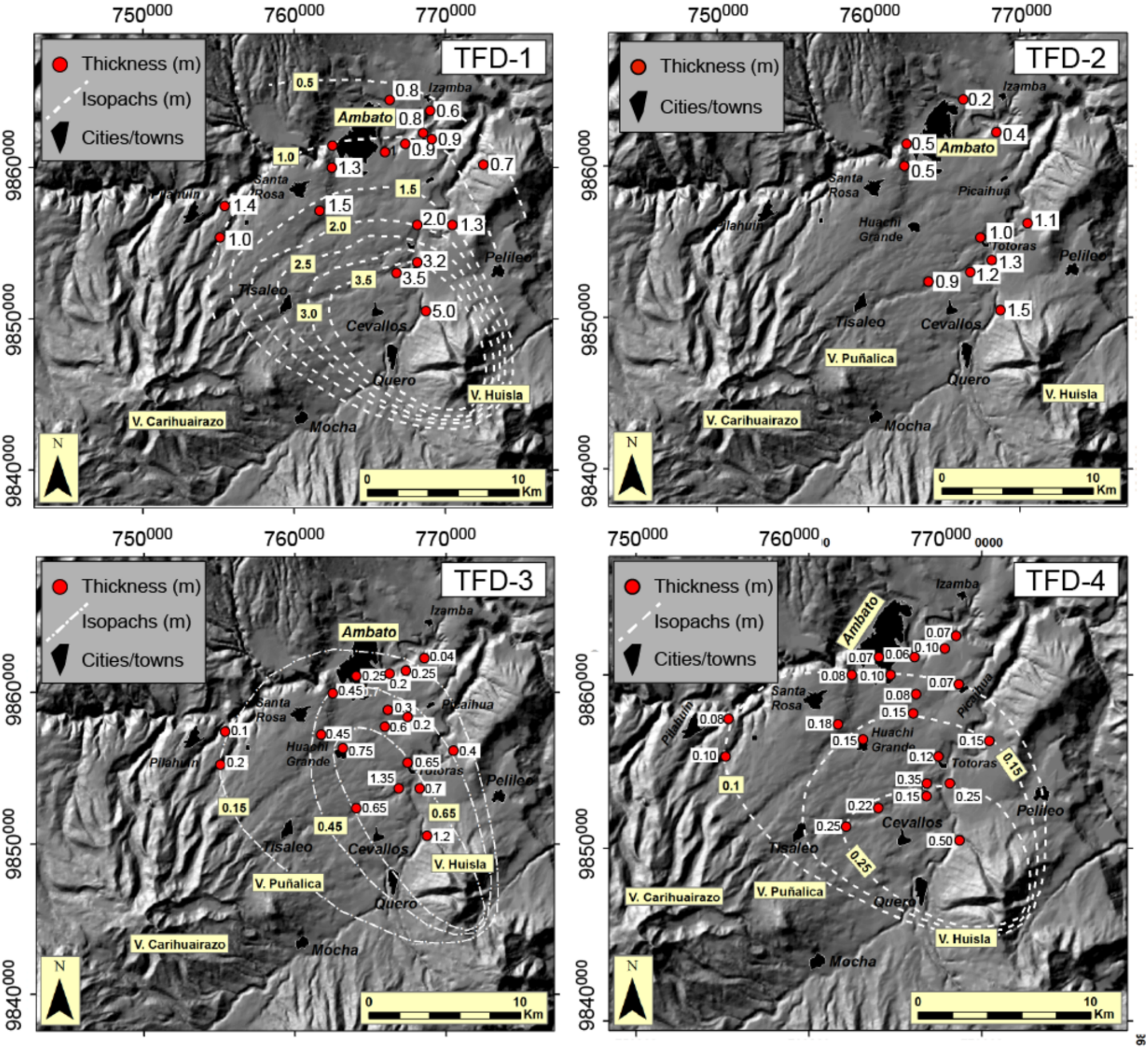

TFD-1
TFD-2
TFD-3
TFD-4
Thickness (m)
Isopachs (m)
Cities/towns
750000
760000
770000
9860000
9850000
9840000
Ambato
Izamba
Santa Rosa
Pilahuin
Picaihua
Huachi Grande
Totoras
Pelileo
Tisaleo
Cevallos
Quero
Mocha
V. Huisla
V. Puñalica
V. Carihuairazo
N
0
10
Km
0.5
1.0
1.5
2.0
2.5
3.0
3.5
0.8
0.8
0.6
0.9
0.9
1
1.3
0.7
1.4
1.5
2.0
1.3
1.0
3.2
3.5
5.0
0.2
0.4
0.5
0.5
1.1
1.0
1.3
1.2
0.9
1.5
0.04
0.25
0.2
0.25
0.45
0.3
0.2
0.6
0.1
0.45
0.75
0.4
0.2
0.65
1.35
0.7
0.65
0.65
1.2
0.15
0.45
0.07
0.10
0.07
0.06
0.08
0.10
0.07
0.08
0.15
0.08
0.18
0.15
0.10
0.15
0.12
0.35
0.25
0.15
0.22
0.25
0.50
0.1
0.15
0.25

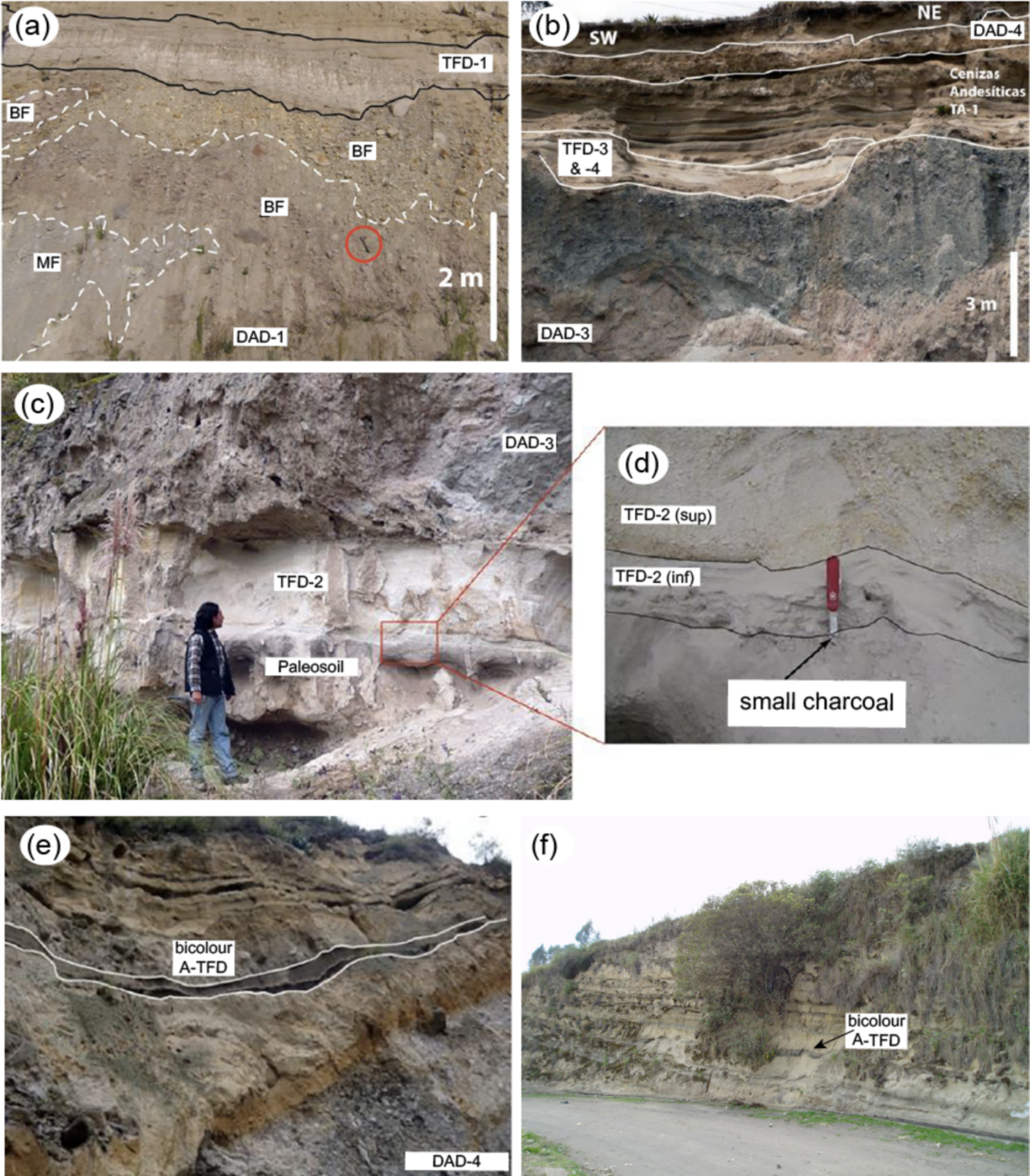
(a)
TFD-1
BF
BF
BF
MF
2 m
DAD-1
(b)
SW
NE
DAD-4
Cenizas Andesíticas TA-1
TFD-3 & -4
3 m
DAD-3
(c)
DAD-3
TFD-2
Paleosoil
(d)
TFD-2 (sup)
TFD-2 (inf)
small charcoal
(e)
bicolour A-TFD
DAD-4
(f)
bicolour A-TFD

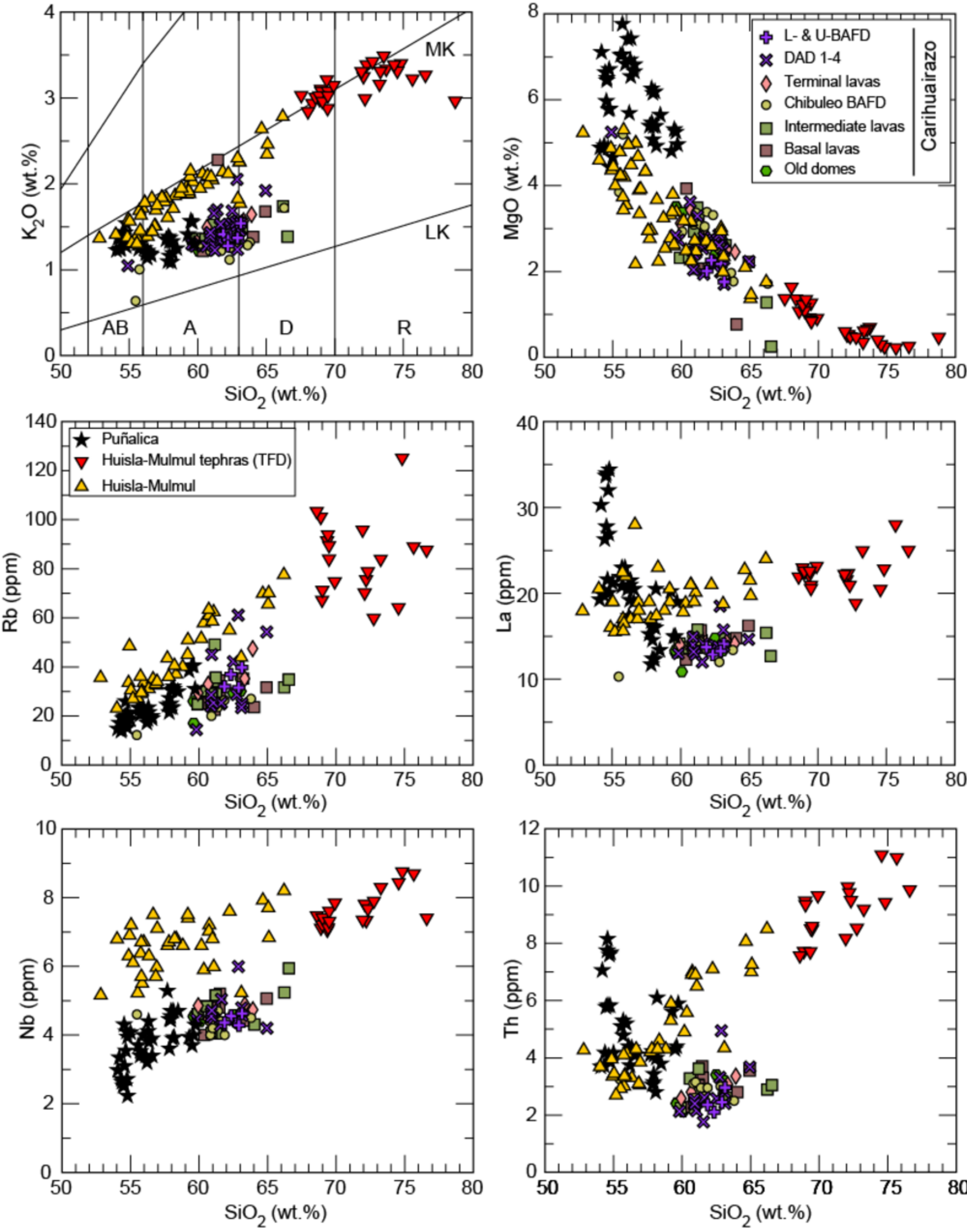
K$_2$O (wt.%)
SiO$_2$ (wt.%)
MK
LK
AB
A
D
R
MgO (wt.%)
L- & U-BAFD
DAD 1-4
Terminal lavas
Chibuleo BAFD
Intermediate lavas
Basal lavas
Old domes
Carihuairazo
Rb (ppm)
Puñalica
Huisla-Mulmul tephras (TFD)
Huisla-Mulmul
La (ppm)
Nb (ppm)
Th (ppm)
0
1
2
3
4
6
8
10
12
20
30
40
60
80
100
120
140
50
55
60
65
70
75
80

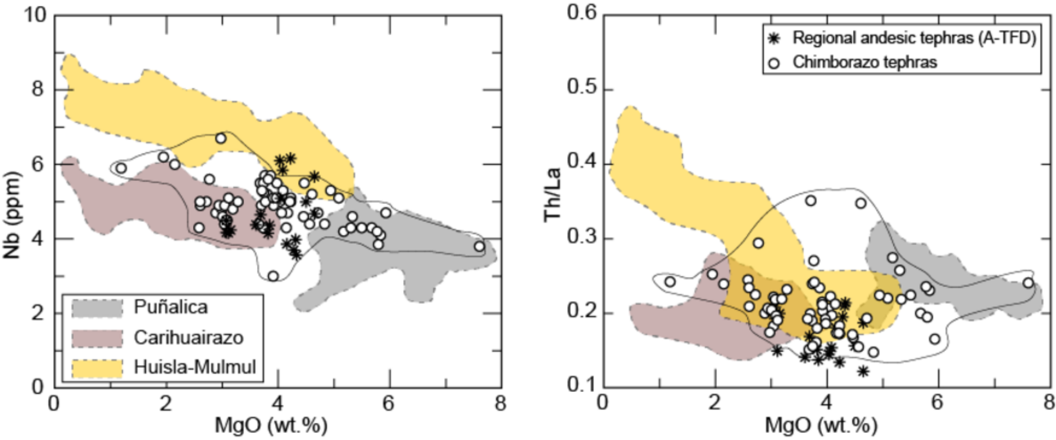
Nb (ppm)
0
2
4
6
8
10
MgO (wt.%)
0
2
4
6
8
Puñalica
Carihuairazo
Huisla-Mulmul
Th/La
0.1
0.2
0.3
0.4
0.5
0.6
MgO (wt.%)
0
2
4
6
8
Regional andesic tephras (A-TFD)
Chimborazo tephras

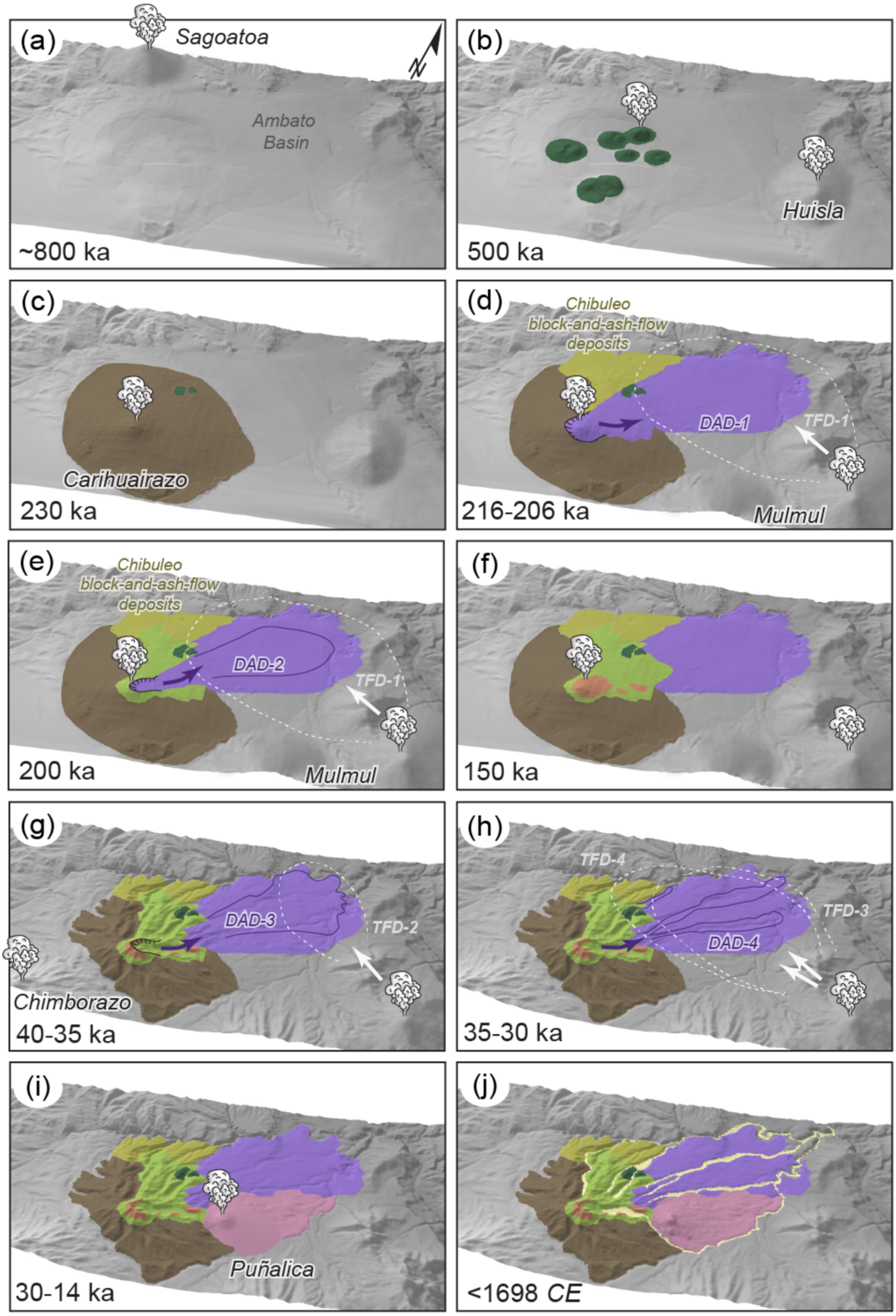
(a)
Sagoatoa
Ambato Basin
~800 ka
(b)
Huisla
500 ka
(c)
Carihuairazo
230 ka
(d)
Chibuleo block-and-ash-flow deposits
DAD-1
TFD-1
Mulmul
216-206 ka
(e)
Chibuleo block-and-ash-flow deposits
DAD-2
TFD-1
Mulmul
200 ka
(f)
150 ka
(g)
DAD-3
TFD-2
Chimborazo
40-35 ka
(h)
TFD-4
TFD-3
DAD-4
35-30 ka
(i)
Puñalica
30-14 ka
(j)
<1698 CE

Sample No.	**CAR14**	**CAR15**	**RIO87A**	**RIO87B**	**RIO117**	**RIO118**	**16EQ45**	**16EQ49**	**16EQ51**	**CAR69**	**16EQ31**	**CAR62A**	**CAR60**	**16EQ48**	**16EQ50**	**CAR13A**	**RIO81A**	**CAR11A**	**CAR09A**	**CAR09C**	**CAR11C**	**17EQ115**
Unit	Old lava domes	Old lava domes	Basal lava flows	Basal lava flows	Basal lava flows	Basal lava flows	Basal lava flows	Intermediate lava flows	Intermediate lava flows	Intermediate lava flows	Intermediate lava flows	Terminal edifice	Terminal edifice	Terminal edifice	Terminal edifice	Chibuleo BAFD	Chibuleo BAFD	DAD	DAD	DAD	BAFD	BAFD
UTM Easting$^+$	753880	753414	747041	747041	754241	753541	751507	748257	749690	750416	753781	754096	755579	748369	749690	754837	746841	761450	763787	763787	761450	759985
UTM Northing$^+$	9851818	9851471	9843725	9843725	9841025	9840625	9845930	9844399	9844487	9850179	9847553	9845243	755579	9855162	9844256	9854964	9854025	9856808	9852012	9852012	9856808	9855162
Location	Sunantza dome	Cruz Maqui dome	Piedra Negra lava flow, SW flank	Piedra Negra lava flow, SW flank	Lava flow, SE flank	Lava flow, SE flank	Río Pachanlica valley lava flow	Lava flow, W flank	BAFD, W flank	Lava flow, N flank	Lava, Punta Tumbuso	Sta Rosa dome	Cerro Pitiunga dome	Young lava flow, W flank	Lava flow, Terminal cone	Chibuleo BAFD	Tundahua BAFD	DAD-1, Bellavista section	DAD-2, El Carmen section	DAD-3, El Carmen section	L-BAFD, Bellavista section	L-BAFD, San Vicente section
SiO2	59.63	62.23	60.70	61.25	61.50	61.20	59.17	60.55	62.03	60.07	60.61	63.68	61.06	59.14	58.94	59.87	60.70	61.29	62.30	61.00	61.45	62.39
TiO2	0.76	0.64	0.71	0.69	0.68	0.75	0.63	0.69	0.58	0.68	0.69	0.60	0.73	0.74	0.67	0.71	0.71	0.60	0.52	0.59	0.58	0.59
Al2O3	17.52	17.31	17.10	17.15	17.65	17.40	16.55	17.15	16.43	18.86	18.03	16.66	16.80	17.21	16.52	16.88	17.08	17.58	17.46	17.19	17.82	17.20
Fe2O3*	6.44	5.57	6.12	5.97	5.73	6.00	6.00	5.96	5.19	6.05	6.34	5.00	6.10	6.54	6.02	5.96	6.18	5.77	5.09	5.25	5.82	5.62
MnO	0.10	0.09	0.09	0.09	0.08	0.09	0.09	0.09	0.08	0.10	0.10	0.08	0.09	0.10	0.09	0.10	0.09	0.10	0.09	0.09	0.10	0.10
MgO	3.51	2.41	2.92	2.85	2.07	2.90	3.86	2.88	2.57	2.33	2.34	2.45	3.48	3.08	3.34	3.12	3.08	2.52	1.68	2.13	2.00	2.16
CaO	6.11	5.01	5.52	5.50	5.35	5.60	6.19	5.82	5.30	5.94	5.99	4.74	5.59	6.06	6.08	5.89	5.92	5.75	5.02	5.24	5.61	5.46
Na2O	4.41	4.58	4.41	4.40	4.50	4.51	4.12	4.17	4.29	4.65	4.38	4.61	4.26	4.28	3.84	4.36	4.46	4.42	4.82	4.24	4.33	4.08
K2O	1.31	1.53	1.47	1.45	2.28	1.43	1.19	1.40	1.46	1.37	1.36	1.64	1.52	1.30	1.45	1.38	1.21	1.33	1.45	1.65	1.40	1.36
P2O5	0.22	0.20	0.20	0.20	0.21	0.20	0.19	0.18	0.18	0.23	0.23	0.16	0.21	0.22	0.18	0.20	0.22	0.20	0.24	0.19	0.23	0.22
LOI	0.12	0.37	0.23	0.21	0.06	0.10	0.71	-0.04	0.13	0.02	0.24	0.00	0.02	-0.08	1.59	1.36	0.22	-0.09	0.72	1.43	0.67	0.58
Total	100.13	99.94	99.47	99.76	100.11	100.18	98.71	98.86	98.25	100.29	100.29	99.61	99.86	98.59	98.73	99.82	99.87	99.46	99.38	99.00	100.00	99.75
Sc	13.17	10.96	10.50	10.50	8.70	10.80	13.98	12.68	9.99	9.47	10.05	8.52	12.30	12.00	13.58	13.19	13.80	10.58	6.67	8.80	8.07	9.02
V	146.54	92.06	137.00	134.00	118.00	133.00	135.44	140.85	116.00	121.47	130.69	106.77	134.09	147.75	177.39	143.59	154.00	123.03	70.52	101.87	99.84	110.36
Cr	53.58	11.55	38.00	38.00	11.00	27.00	116.10	19.37	27.03	4.76	6.10	37.96	73.51	26.59	47.03	39.96	42.00	12.78	4.09	10.39	5.88	11.41
Co	20.72	15.00	16.00	19.00	13.00	17.00	18.43	16.32	14.44	14.89	16.03	15.01	19.61	18.38	19.50	17.09	18.00	14.61	9.25	12.75	12.10	14.70
Ni	46.72	18.76	36.00	28.00	10.00	29.00	65.63	27.77	25.86	7.64	7.52	29.25	47.83	32.79	41.45	33.34	38.00	18.39	4.88	9.78	5.53	9.20
Rb	17.03	29.36	29.50	29.00	34.50	22.50	25.23	32.32	35.30	24.80	30.22	47.46	49.07	29.37	32.96	24.83	20.00	24.87	24.95	42.16	32.00	31.55
Sr	692.38	598.99	604.00	608.00	666.00	645.00	584.10	586.01	609.68	712.66	677.36	571.88	597.45	602.18	595.16	749.79	795.00	604.77	650.07	609.99	664.67	649.86
Y	11.41	11.95	12.20	12.00	11.70	13.00	12.73	11.94	9.99	12.83	11.91	9.02	10.47	13.13	11.37	12.93	12.00	11.74	11.39	11.37	11.96	10.86
Zr	104.51	77.02	116.00	132.00	123.00	112.00	97.80	108.64	39.60	111.41	113.13	65.36	101.94	114.69	106.40	95.95	83.00	78.41	86.81	98.36	105.98	94.24
Nb	4.56	4.60	4.70	5.20	4.80	4.80	4.00	4.08	4.41	4.61	4.84	4.74	4.39	4.85	4.48	4.39	4.00	4.28	4.57	4.45	4.36	4.28
Ba	610.68	709.74	662.00	685.00	628.00	670.00	614.06	669.87	836.43	593.08	598.15	705.67	668.03	614.39	661.57	581.14	615.00	593.93	655.49	668.36	592.90	626.59
La	13.06	14.78	14.50	14.50	15.70	15.00	12.27	14.80	14.69	14.16	13.66	14.16	13.66	14.02	13.70	13.76	14.00	12.00	13.87	13.93	13.74	13.29
Ce	26.87	32.11	30.50	31.00	30.00	30.50	23.25	29.85	30.72	29.65	29.28	26.33	30.37	28.13	27.65	27.76	29.00	27.01	29.97	30.99	31.17	28.48
Nd	15.52	15.77	17.00	17.00	17.00	17.50	13.74	15.92	14.56	16.93	15.62	14.33	14.77	16.72	14.61	16.09	16.00	13.80	15.66	15.04	15.68	14.13
Sm	3.46	3.21	3.40	3.35	3.70	3.70	2.88	3.22	2.97	3.58	3.24	2.88	3.04	3.45	3.16	3.41	3.35	2.92	3.38	3.19	3.59	2.93
Eu	1.02	1.01	1.02	1.03	0.98	1.03	0.82	0.96	0.93	1.09	1.03	0.82	0.97	1.17	0.78	0.96	0.99	0.85	1.00	0.92	1.04	0.95
Gd	2.87	3.36	3.20	3.20	3.00	3.50	2.61	2.36	2.68	3.00	3.39	2.36	3.09	3.06	2.42	3.08	3.20	3.01	3.16	3.10	3.32	2.60
Dy	2.06	1.98	2.20	2.20	2.15	2.35	2.15	2.29	1.77	2.24	2.09	1.71	1.93	2.44	2.06	2.16	2.15	1.95	1.86	2.06	2.12	2.01
Er	0.32	0.03	1.15	1.10	1.10	1.20	1.14	1.24	0.85	0.38	1.00	0.00	-0.01	1.15	0.77	0.79	1.10	-0.04	0.14	-0.05	-0.03	1.25
Yb	0.97	1.08	1.05	1.02	0.97	1.12	1.00	0.88	0.59	1.14	1.02	0.72	0.95	0.92	0.80	1.16	0.98	1.09	1.01	0.99	1.07	0.96
Th	2.43	3.41	3.30	3.30	3.70	3.00	2.29	3.04	2.60	2.25	3.28	3.36	2.91	2.58	2.80	2.58	2.60	1.77	2.40	2.58	2.36	2.45

$^+$ WGS84, 17 zone

* all Feo as Fe2O3

Sample	Unit	Location	UTM Easting	UTM Northing	Phase	K (%)	^{40}Ar* (%)	^{40}Ar* x 10^{11} (at/g)	**Age ± 1σ** (ka)	Mean age (ka)
16EQ45	Basal lava flows	Lava flow, inside the avalanche scar, NE flank	751,507	9,845,930	Groundmass	1.152	2.80	2.5938	216 ± 8	217 ± 9
							2.59	2.6197	218 ± 9	
17EQ115	L-DAFD	Juvenile block from a block-and-ash-flow deposit	759,985	9,855,162	Groundmass	1.741	3.73	3.7811	208 ± 4	206 ± 4
							6.16	3.7181	204 ± 4	
16EQ49	Basal lava flows	Proximal lava flow/dome, W flank	748,257	9,844,399	Groundmass	1.682	4.89	3.5067	200 ± 5	199 ± 5
							4.69	3.4962	199 ± 5	
16EQ51	Basal lava flows	Juvenile block from a summit block-and-ash-flow	749,690	9,844,487	Groundmass	1.471	3.07	3.0723	200 ± 7	198 ± 7
							2.78	3.0216	197 ± 8	
16EQ31	Basal lava flows	Lava flow, NE flank	753,781	9,847,553	Groundmass	1.463	7.17	3.0679	201 ± 4	197 ± 4
							9.29	2.9641	194 ± 3	
					Plagioclase	0.356	2.22	0.7029	189 ± 9	187 ± 9
							2.18	0.6837	184 ± 9	
CAR69	Basal lava flows	Lava flow, N flank	750,425	9,850,188	Groundmass	1.322	6.11	2.5872	187 ± 4	186 ± 5
							3.97	2.5833	187 ± 5	
							5.15	2.5392	184 ± 4	
					Plagioclase	0.377	1.87	0.7212	183 ± 10	178 ± 11
							1.60	0.6760	172 ± 11	
CAR60	Terminal edifice	Pitiunga lava dome, E flank, Pachanlica valley	755,588	9,845,772	Groundmass	1.663	6.89	3.0625	176 ± 4	176 ± 10
							5.34	3.2221	185 ± 4	
							4.45	2.8672	165 ± 4	
16EQ50	Terminal edifice	Lava flow, summit pyramide	749,690	9,844,256	Groundmass	1.852	2.60	3.3111	171 ± 7	172 ± 7
							2.45	3.3279	172 ± 7	
16EQ48	Terminal edifice	Juvenile fragment of dome breccia	748,369	9,855,162	Groundmass	1.473	3.08	2.5013	163 ± 6	157 ± 5
							3.33	2.3463	153 ± 5	

Sample No.	Lab code	Locality	UTM Easting	UTM Northing	Unit	Sample type	^{14}C age (years BP)
CAR-09M	GrA 46688	El Carmen	763787	9852012	Paleosoil below TFD-2	charcoal	39030 +440/-380
CAR-09N	GrA 48843	El Carmen	763787	9852012	Paleosoil below TFD-2	charcoal	> 45000
CAR-10F	GrA 48875	San Vicente	760098	9855155	L-BAFD	charcoal	> 45000

		Age max.	Age min.	Duration	Raw volume	Total volume	Eruptive rate		Erosion rate	
		ka	ka	ka	km^3	km^3	km^3/kyr	mm/yr	km^3/kyr	mm/yr
Construction phase of Carihuairazo	Without erosion correction	223 ± 6*	157 ± 5	66 ± 8	85 ± 49		1.3 ± 0.8	5.3 ± 3.1		
	Considering eroded volume during the construction	223 ± 6*	157 ± 5	66 ± 8		97 ± 53	1.5 ± 0.9	6.1 ± 3.6		
Erosion phase	Since the end of Carihuairazo construction	157 ± 5	0	157 ± 5	18 ± 5				0.12 ± 0.03	0.48 ± 0.13
	Considering eroded volume during the construction	157 ± 5	0	157 ± 5		30 ± 9			0.14 ± 0.04	0.56 ± 0.16
	Volume eroded during the construction	223 ± 6	157 ± 5	66 ± 8		12 ± 4				